1 **A Synthesis of Global Streamflow characteristics, Hydrometeorology, and**

2 **catchment Attributes (GSHA) for Large Sample River-Centric Studies**

4 Ziyun Yin[1], Peirong Lin[1,2*], Ryan Riggs[3], George H. Allen[4], Xiangyong Lei[1], Ziyan

5 Zheng[5,6], Siyu Cai[7]

6 1. Institute of Remote Sensing and GIS, School of Earth and Space Sciences, Peking University

7 2. International Research Center for Big Data for Sustainable Development Goals, Beijing, China

8 3. Department of Geography, Texas A&M University, Texas, USA

9 4. Department of Geosciences, Virginia Polytechnic Institute and State University, Virginia, USA

10 5. Key Laboratory of Regional Climate-Environment Research for Temperate East Asia, Institute of

11   Atmospheric Physics, Chinese Academy of Sciences, Beijing, China

12 6. University of Chinese Academy of Sciences, Beijing, China

13 7. State Key Laboratory of Simulation and Regulation of Water Cycle in River Basin, China Institute

14   of Water Resources and Hydropower Research, Beijing, China

15 * *Correspondence to*: Peirong Lin (peironglinlin@pku.edu.cn)

16 ~~Manuscript~~Revised manuscript submitted to *ESSD, ~~July 1st~~November 15th, 2023*

Abstract

18   Our understanding and predictive capability of streamflow processes largely rely on high-

19 quality datasets that depict a river's upstream basin characteristics. Recent proliferation of large

20 sample hydrology (LSH) datasets has promoted model parameter estimation and data-driven

21 analyses of the hydrological processes worldwide, yet existing LSH is still insufficient in terms of

22 sample coverage, uncertainty estimates, and dynamic descriptions of anthropogenic activities. To

23 bridge the gap, we contribute the Synthesis of Global Streamflow characteristics, Hydrometeorology,

24 and catchment Attributes (GSHA) to complement existing LSH datasets, which covers 21,568

25 watersheds from 13 agencies for as long as 43 years based on discharge observations scraped from

26 web. In addition to annual and monthly streamflow indices, each basin's daily meteorological

27 variables (i.e., precipitation, 2 m air temperature, longwave/shortwave radiation, wind speed, actual

28 and potential evapotranspiration), daily-weekly water storage terms (i.e., snow water equivalence,

29 soil moisture, groundwater percentage), and yearly dynamic descriptors of the land surface

30 characteristics (i.e., urban/cropland/forest fractions, leaf area index, reservoir storage and degree of

31 regulation) are also provided by combining openly available remote sensing and reanalysis datasets.

32 The uncertainties of all meteorological variables are estimated with independent data sources. Our

33 analyses ~~revealed~~reveal the following insights: (i) the meteorological data uncertainties vary across

34 variables and geographical regions, and the ~~prominent patterns~~ revealed pattern should be accounted

35 for by LSH users, (ii) ~6% watersheds shifted between human managed and natural states during

36 ~~the GSHA time span~~2001-2015, e.g., basins with environmental recovery projects in Northeast

37 China, which may be useful for hydrologic analysis that takes the changing land surface

38 characteristics into account, and (iii) GSHA watersheds ~~observed~~showed a more widespread

39 declining trend in runoff coefficient than an increasing trend, pointing towards critical water

40 availability issues. Overall, GSHA is expected to serve hydrological model parameter estimation

41 and data-driven analyses as it continues to improve. ~~GSHA v1.0 can be accessed at~~
42 ~~*https://doi.org/10.5281/zenodo.8090704*~~GSHA v1.1 can be accessed at
43 *https://doi.org/10.5281/zenodo.8090704* and *https://doi.org/10.5281/zenodo.10127757.* (Yin et al.,
44 2023).

1 Introduction

46   Climate change has posed profound challenges to the management of freshwater resources,
47 specifically riverine floods or water shortages (AghaKouchak et al., 2020; Thackeray et al., 2022).
48 The urgent need for flood and drought forecasting, water resources planning and management, all
49 call for high-quality streamflow predictions for basins worldwide to analyse global terrestrial water
50 conditions in a systematic view (Burges, 1998). The scarcity of hydrological observations has
51 brought challenges to these predictions (Belvederesi et al., 2022; Hrachowitz et al., 2013), thus the
52 development of computer models that allow for "modelling everything everywhere" (Beven &
53 Alcock, 2012) constitutes the backbone of hydrological studies. Existing studies have used
54 physically-based and data-driven models for streamflow simulation (Lin et al., 2018; Nandi &
55 Reddy, 2022; Zhang et al., 2020), with efforts to improve accuracy of prediction by combining both
56 (Cho & Kim, 2022; Razavi & Coulibaly, 2013). Yet the prediction of the magnitude, timing, and
57 trend of critical streamflow characteristics are still subject to multiple sources of errors and
58 uncertainties (Bourdin et al., 2012; Brunner et al., 2021).
59   Streamflow (Q) can be represented by the simple water balance equation involving
60 precipitation (P), evapotranspiration (ET), and water storage terms (S) denoted as $Q = P - ET - \Delta S$,
61 yet influencing factors of these components could bring uncertainties that ~~will~~ cascade downstream.
62 Starting from the model assumptions to the data used to represent climate, soil water, ice cover,
63 topography and land use, as well as ~~to~~ the less well-known processes such as human perturbations
64 and sub-surface flows (Benke et al., 2008; Wilby & Dessai, 2010), these complications impede our
65 understanding of streamflow processes across scales, which also limits the modelling and predictive
66 capability for streamflow. Thus, reducing the predictive uncertainties ~~require~~requires high-quality
67 data with massive samples capable of depicting each of the water balance components, as well as
68 the natural and anthropogenic factors involved (Gupta et al., 2014).
69   Efforts have been made to address the need ~~of~~for such kind of high-quality datasets on
70 watershed-scale hydro-climate and environmental conditions during the past couple of decades. One
71 of the earliest was the most widely used dataset generated for the Model Parameter Estimation
72 Experiment (MOPEX) project aimed at better hydrological modelling (Duan et al., 2006). Historical
73 hydro-meteorological data and land surface characteristics for over 400 hydrologic basins in the
74 United States were provided, which was fundamental to the progress in large sample hydrology
75 (LSH) (Addor et al., 2020; Schaake et al., 2006). Later the dataset was expanded to 671 catchments
76 in the contiguous United States (CONUS) and benchmarked by model results (Newman et al., 2015).
77 Based on these studies, the Catchment Attributes and Meteorology for Large-sample Studies
78 (CAMELS) dataset was developed, providing comprehensive and updated data on topography,
79 climate, streamflow, land cover, soil, and geology attributes for each catchment (Addor et al., 2017).

The CONUS CAMELS dataset soon became influential in LSH and has since inspired researchers from Australia (Fowler et al., 2021), Europe (Coxon et al., 2020; Delaigue et al., 2022; Klingler et al., 2021), South America (Alvarez-Garreton et al., 2018; Chagas et al., 2020), and China (Hao et al., 2021) to contribute their regional CAMELS. Another comprehensive regional LSH dataset for North America named the Hydrometeorological Sandbox - École de Technologies Supérieure (HYSETS) dataset, ~~is~~was also developed with larger sample size (14425 watersheds) and richer data sources compared with the CAMELS (Arsenault et al., 2020).

While these datasets are reliable data sources for regional studies, attempts on building global datasets ~~has~~have become the new norm in the era of big data to boost our analytical and modelling capability for the terrestrial hydrological processes. The HydroATLAS dataset ~~integrates~~integrated indices of hydrology, physiography, climate, land cover, soil, geology, and anthropogenic activity attributes for 8.5 million global river reaches (Lehner et al., 2022; Linke et al., 2019). A recent work combined a series of CAMELS ~~dataset~~datasets with HydroATLAS attributes into a new global community dataset on the cloud named Caravan, with dynamic hydro-climate variables and comprehensive static catchment attributes extracted on 6830 watersheds (Kratzert et al., 2023), which represents by far the most comprehensive synthesis of existing CAMELS. Another global-scale effort, the Global Streamflow Indices and Metadata archive (GSIM), incorporated dynamic streamflow indices and attribute metadata for topography, climate type, land cover, etc., for over 35000 gauges (Do et al., 2018; Gudmundsson et al., 2018), and the streamflow indices ~~are~~were updated to allow for trend analysis (Chen et al., 2023). A recent study filled in the discontinuity and latency of gauge records, and provided streamflow for over 45,000 gauges with improved data quality (Riggs et al., 2023). These global-scale datasets have been widely used in data-driven machine learning models (Kratzert et al., 2019a, 2019b; Ren et al., 2020), physical hydrological models (Aerts et al., 2022; Clark et al., 2021), and parameter estimation and regionalization studies (Addor et al., 2018; Fang et al., 2022).

Although the flourishment of LSH datasets has promoted comparative hydrological studies (Kovács, 1984) and large-scale hydrological modeling and ~~analyses~~analysis efforts, several challenges are still standing in the way ~~to realize~~of realizing the full potential of LSH. As briefly outlined in a recent review by Addor et al. (2020), current LSH datasets lack common standards, metadata and uncertainty estimates, and are insufficient in characterising human interventions. More specifically, the following major critical aspects still need ~~attentions~~attention from the LSH developers, which we attempt to address with GSHA (Yin et al., 2023). First, the majority of current datasets (especially those at a global scale) ~~incorporate~~incorporated only one data source for each variable, while earth observations, reanalysis, satellite-based estimates are subject to uncertainties (Merchant et al., 2017; Ukhurebor et al., 2020). These uncertainties were rarely represented and may bring difficulties to the regionalization of model parameters (Beck et al., 2016), while also resulting in inconsistent conclusions. Second, anthropogenic activities including land use and land cover (LULC) changes, dam and reservoir building, etc., are critical drivers of shifts in streamflow statistical moments (Niraula et al., 2015). However, historical time series of watershed human modifications ~~have~~were rarely ~~been~~ included in LSH datasets, which is particularly problematic for regions with rapid economic growth. Finally, although the most recent Caravan ~~has~~ provided hydroclimate data for global watersheds, the samples are limited to the existing regional CAMELS which Caravan synthesizes. Therefore, plenty of room is left to increase data sample size and spatial coverage by revisiting the streamflow data acquisition process in a more comprehensive way.

124   To complement existing LSH datasets, we contribute the first version of a synthesis of Global
125 Streamflow characteristics, Hydrometeorology, and catchment Attributes (GSHA v_1.0) for large-
126 sample river-centric studies. GSHA features the following characteristics:

127 ● Updated physical and anthropogenic descriptors of global rivers, covering streamflow
128   characteristics, hydrometeorological variables, and land use land cover changes for 21568
129   watersheds derived from gauged streamflow records from 13 agencies.
130 ● Streamflow indices for data scarce regions, including those derived from 263 gauges in
131   China, are included.
132 ● Extended temporal coverage for as long as 43 years (1979-2021), which varies regionally.
133 ● Uncertainty estimates for the meteorological variables.
134 ● Dynamic descriptors for the urban, forest, and cropland fractions, as well as reservoir
135   storage capacity to improve the representation of human activities in the basin.

136   With the above features, we expect GSHA to support hydrological model parameter estimation
137 and data-driven analysis of global streamflow as one of the most comprehensive LSH datasets
138 regarding sample size, variable dynamics, and uncertainty estimates. **Table 1** summarizes the
139 differences between GSHA and other prominent LSH datasets. Our paper is organized as follows.
140 Section 2 expands on **Table 1** and ~~provide~~provides more details of the data included for GSHA.
141 Section 3 introduces the data sources and methodologies involved in creating GSHA. Section 4
142 highlights the key features of GSHA by conducting some analyses, followed by conclusions reached
143 in Section 5.
144
145 **Table 1 Comparison of GSHA with other LSH datasets.** Note that we only include the CONUS
146 CAMELS dataset to represent regional LSH datasets for this comparison, as other regional CAMELS
147 share large similarity with CONUS CAMELS.

Factors	CAMELS (eg. US)	HydroATLAS	Caravan	GSIM	GSHA
Spatial extent	Regional	Global	Global	Global	Global
Sample size	671	8.5 million	6830	35002	21568
Time span	1980–2015	Static	1981–2020	1806-2016	1979-2021
Streamflow dynamics	Yes	No	Yes	Yes (statistical indices)	Yes (monthly and yearly statistical indices)
Meteorological time series	Yes	No	Yes	No	Yes
Multi data sources for meteorological variables	Yes	No	No	No	Yes (**with uncertainty estimates**)
Water storage dynamics	No	No	Only soil water dynamics	No	**Yes**
Land cover dynamics	No	No	No	No	**Yes**

Reservoir dynamics	No	No	No	No	**Yes**
Static attributes	Yes	Yes	Yes (from HydroATLAS)	Yes	Yes (from HydroATLAS)

2 Dataset content of GSHA v1

149   In this section, the data fields, variables, and attributes included in GSHA are described in more
150   details and summarized in **Table 2**. For the instructions of the data format, we ~~provided~~provide a
151   user manual along with the dataset (see readme.docx). GSHA includes yearly and monthly
152   streamflow characteristics derived from daily discharge observations, meteorological variables
153   (including precipitation, 2-m air temperature, long- and shortwave radiation, wind speed, actual and
154   potential evapotranspiration (AET and PET)), daily or weekly water storage terms (4 layers of soil
155   moisture, groundwater, and snow depth water equivalence), daily vegetation index (leaf area index
156   (LAI)), yearly LULC characteristics (urban, cropland, and forest fraction), and yearly reservoir
157   information (degree of regulation (DOR) and reservoir capacity). For each meteorological variable,
158   multiple independent data sources are incorporated to provide uncertainty estimates. Static attributes
159   like land physiography, soils, and geology are not additionally extracted, as similar efforts have been
160   made by other researchers, so we directly matched our gauge locations to the HydroATLAS dataset
161   (Lehner et al., 2022; Linke et al., 2019) by providing the river ID match table. Users can link the
162   two to obtain these attributes.

163   **Watershed polygons:** GSHA includes 21568 watershed polygons delineated from the global
164   gauges, which ~~is~~are stored as Esri Shapefile format. The ID and agency of each watershed is the
165   same as the corresponding gauge ID, and the gauge latitude/longitude are in decimal degree. The
166   area denotes the upstream drainage ~~basin~~ area of the gauge. Some of the IDs contain characters
167   (such as '.', '-', etc.) inconsistent with the majority of IDs. For the convenience of the users, we
168   unified these as underscores and stored the new file names as 'filename'. We also provide
169   independent files summarizing basic information of the watersheds, including matched MERIT
170   river reach COMID, upstream area, order and downstream river reach COMID, as well as
171   verification with officially reported areas of the agencies.

172   **Streamflow indices:** GSHA publishes annual and monthly streamflow indices derived from
173   daily streamflow data, including different percentiles, and mean/median/minimum/maximum. The
174   frequency and durations of extremely high and low streamflow events are also provided~~, along with~~.
175   We also include numbers of zero observations and valid samples to allow ~~extreme streamflow~~
176   ~~analysis and~~ flexible data screening by the users. The indices are stored as comma-~~-~~separated values
177   (CSV) files ~~by year~~, with each watershed corresponding to one file. A complementary R package
178   can be used to automatically download many of the gauge datasets is available at
179   ~~https://github.com/Ryan-Riggs/RivRetrieve~~https://github.com/Ryan-Riggs/RivRetrieve (Riggs et
180   al., 2023).

181   **Meteorological variables:** The meteorological variables selected are the most influential

drivers for streamflow, which ~~includes~~include precipitation, 2-m temperature, ET, radiation and wind speed. In main-stream land surface models, ET is a diagnostic variable derived from meteorological inputs and is not considered as meteorological forcing. However, as many hydrological models also use potential ET as an input variable, and model calibration sometimes involves actual ET (Immerzeel & Droogers, 2008), we include the two variables and place ~~it~~them into the meteorological variable category. For each variable, more than one data sources are used to allow for uncertainty analysis, which ~~will be~~is provided on a yearly basis in an independent file.

Natural water storage terms and land use/land cover change: These include soil moisture, snow water equivalent, and ~~ground water~~groundwater percentages. We also include yearly land cover dynamics (i.e., urban, forest, and cropland fraction changes), as well as dynamically changing reservoir capacity and degree of regulation (DOR) percentage. Leaf area index (LAI) is also included to reflect the seasonal changes in vegetation canopy that ~~is~~are also key to the streamflow processes.

Static attributes: GSHA does not extract updated static attributes because HydroATLAS already ~~make~~made substantial efforts in this regard. Instead, the listed categories are those mostly related to streamflow prediction from HydroATLAS selected to be included in GSHA files, and we direct the readers to the ID match table to access the entire 281 static attributes offered by HydroATLAS (Lehner et al., 2022; Linke et al., 2019). Our user manual, available at the dataset download site, also provides more information on it.

Table 2 Fields provided with GSHA.

Category	Field	Description	Unit
Watershed Polygons and basic information	Sttn_Nm	The ID of the watershed.	NaN
	Latitude	Latitude of the gauge.	Degree
	Longitude	Longitude of the gauge.	Degree
	Shedarea	The area of delineated watershed.	Km^2
	Agency	The agency the gauge belongs to.	NaN
	filename	The name of the corresponding Shapefile in the dataset.	NaN
	~~filename~~verification	~~The name of the corresponding Shapefile in the dataset.~~Verification of watershed area with officially reported area of the corresponding agency. If we did not access the officially reported area of the watershed on the agency website, the field would be "unverified".	NaN
	COMID	ID of the MERIT river reach matching with the watershed.	NaN
	uparea	Upstream area of the river reach included in the MERIT database.	NaN
	order	Stream order of the river reach.	NaN
	NextDownID	ID of the downstream river reach in	NaN

MERIT.

Category	Indices	Description	Unit/Format
Streamflow indices (yearly)	percentiles	Annual 1, 10, 25, 75, 90, 99 percentiles of daily streamflow.	m³/s
	mean	Annual mean of daily streamflow.	m³/s
	median	Annual median of daily streamflow.	m³/s
	annual maximum flood (AMF)	Annual maximum of daily streamflow.	m³/s
	AMF occurrence date	The date of AMF occurrence.	Year/month/day
	frequency of high-flow events	Number of days in a year with streamflow >= 90 percentile flow.	Days/year
	average duration of high-flow events	Average number of consecutive days >= 90 percentile flow.	Days
	frequency of low-flow events	Number of days in a year with streamflow <= 10 percentile flow.	Days/year
	average duration of low-flow events	Average number of consecutive days <= 10 percentile flow.	Days
	Q=0 days	Number of days with runoff=0.	Days
	valid observation days	Number of days with no missing data. (Valid observations refer to non-null measurements.)	Days

Category	Indices	Description	Unit/Format
Streamflow indices (monthly)	percentiles	Monthly 1, 10, 25, 75, 90, 99 percentiles of daily streamflow.	m³/s
	mean	Monthly mean of daily streamflow.	m³/s
	median	Monthly median of daily streamflow.	m³/s
	monthly maximum flood (MMF)	Monthly maximum of daily streamflow.	m³/s
	MMF occurrence date	The date of MMF occurrence.	Year/month/day
	frequency of high-flow events	Number of days in a month with streamflow >= yearly 90 percentile flow.	Days/month
	average duration of high-flow events	Average number of consecutive days in the month >= yearly 90 percentile flow.	Days
	frequency of low-flow events	Number of days in a month with streamflow <= yearly 10 percentile flow.	Days/month
	average duration of low-flow events	Average number of consecutive days in the month <= yearly 10 percentile flow.	Days
	Q=0 days	Number of days with runoff=0.	Days
	valid observation days	Number of days with no missing data.	Days
Category	**Variable**	**Data source name**	**Unit**

Meteorological Variables	Precipitation	MSWEP	mm
		EM-Earth	mm
	2 m temperature	ERA5	K
		MERRA-2	K
		EUSTACE	K
	Actual evapotranspiration	REA	mm
		GLEAM	mm
	Potential evapotranspiration	GLEAM	mm
		hPET	mm
	Radiation (longwave)	ERA5 land surface net thermal radiation	W/m^2
		MERRA-2 surface net downward longwave flux	W/m^2
	Radiation (shortwave)	ERA5 land surface net solar radiation	W/m^2
		MERRA-2 surface net downward shortwave flux	W/m^2
	10 m wind speed (u component)	ERA5 land u-component of wind	m/s
		MERRA-2 10 metre eastward wind	m/s
	10 m wind speed (v component)	ERA5 land v-component of wind	m/s
		MERRA-2 10 metre northward wind	m/s
	10 m wind speed (actual)	ERA5 land u- and v-components of wind	m/s
		MERRA-2 10 metre northward and eastward wind	m/s

Category	Variable	Data source name	Unit
Water storage terms	Soil moisture layer 1	ERA5 land soil water layer 1 (0-7 cm, 0cm refers to the surface)	m^3/m^3
	Soil moisture layer 2	ERA5 land soil water layer 2 (7-28 cm)	m^3/m^3
	Soil moisture layer 3	ERA5 land soil water layer 3 (28-100 cm)	m^3/m^3
	Soil moisture layer 4	ERA5 land soil water layer 4 (100-289 cm)	m^3/m^3
	Snow water equivalent	ERA5 land snow depth water equivalent	m of water equivalent
	Ground water	GRACE-FO data assimilation	%

Category	Variable	Data source name	Unit
Land use and land cover	Urban fraction	GAUD	%
	Forest fraction	MCD12Q1	%
	Cropland fraction	MCD12Q1	%
	Reservoir capacity	GeoDAR	Million m^3
	DOR	GeoDAR	%
	LAI	CDR LAI	NaN

Category	Attribute	Column name **(directly from**	Unit

		RiverATLAS)	
Static-Physiography	Elevation	ele_mt_uav	m. a.s.l.
	Terrain slope	slp_dg_uav	degrees (x10)
	Stream gradient	sgr_dk_rav	decimetres per km
Static-Hydrology	Inundation Extent	inu_pc_ult	%
	Groundwater Table Depth	gwt_cm_cav	cm
Static-Landcover	Land Cover Classes	glc_cl_cmj	NaN
	Potential Natural Vegetation Classes	pnv_cl_cmj	NaN
	Wetland Extent	wet_pc_u01-u09	%
	Glacier Extent	gla_pc_use	%
	Permafrost Extent	prm_pc_use	%
Static-Soil & geology	Clay Fraction in Soil	cly_pc_uav	%
	Silt Fraction in Soil	slt_pc_uav	%
	Sand Fraction in Soil	snd_pc_uav	%
	Lithological Classes	lit_cl_cmj	NaN
	Soil Erosion	ero_kh_uav	kg/hectare per year

3 Data sources and methodology

3.1 Technical workflow in creating GSHA

The creation of GSHA starts from revisiting the data compilation process for the stream gauging observations from 13 international agencies. The general workflow of GSHA data production processes is illustrated in **Figure 1**, which consists of watershed delineation, variable extraction from both grid and non-grid data sources, and uncertainty analysis.

First, we delineated the upstream watersheds using gauge locations. Calibration of gauge longitudes and latitudes were conducted to match the gauges with the MERIT river network exactly. The delineated watersheds were selected and manually checked using standards of area, topology correctness, and observation data lengths. The selected watersheds went on to be overlayed with grid and non-grid variable data sources for to obtain GSHA variables.
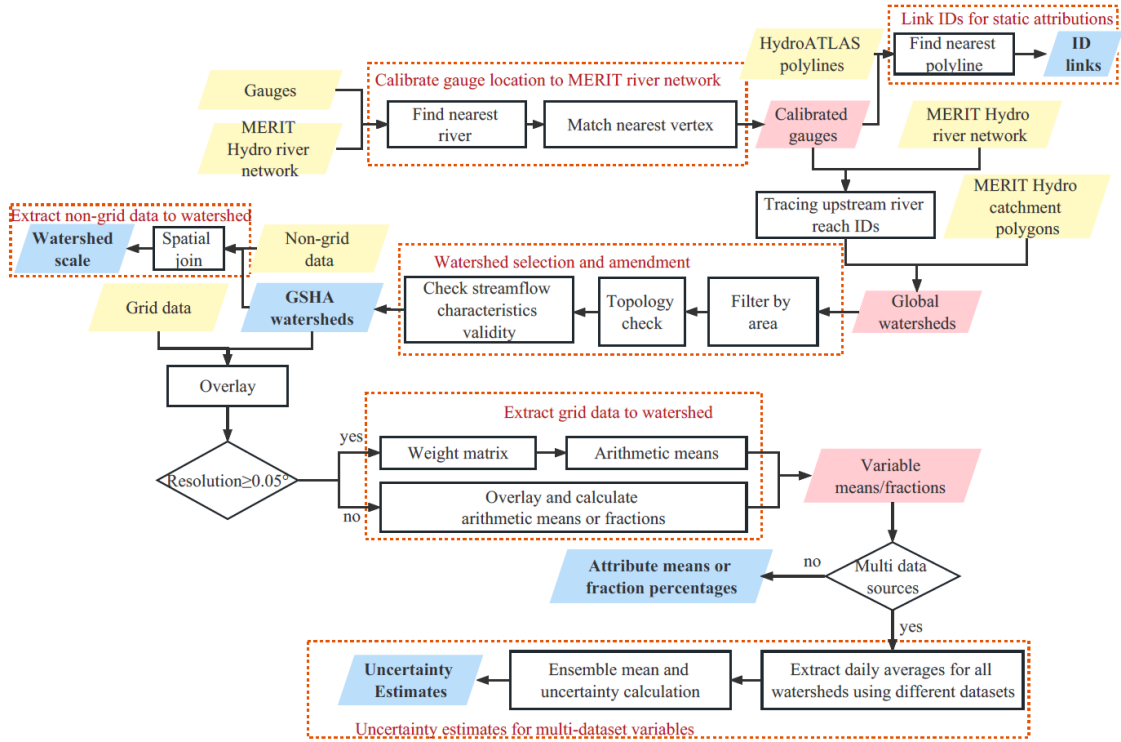
Figure 1 General workflow of GSHA. The yellow parallelograms are the input datasets, the blue ones are the final outputs of GSHA dataset, and the pink ones are the results in the process. The black quadrilaterals represent the extraction and calculation processes, and the red dotted rectangles illustrate different modules of the extraction process.

3.2 Gauge-based streamflow indices

As shown in **Table 3**, in total ~~streamflow data from~~ 36497 gauges were initially scraped from ~~the~~ web and from the Chinese National Real-time Rain and Water Situation Database ~~including the real-time water level and streamflow data of the hydrological stations.~~. For gauges located within ~100- m of each other, those with ~~shorter record lengths are~~fewer years of measurements were removed, assuming that they are redundant with one another. The gauge measurements were converted to a consistent unit (m^3/s) and ~~were~~ then manually compared with GRDC measurements to ensure accurate unit conversion (Riggs et al., 2023). Gauge databases compiled in this study are available through a variety of web interfaces, except for the ~~CHP~~Chinese Hydrology Project (CHP) data which is provided by the authors of the dataset (Henck et al 2010, Schmidt et al 2011), and processed into annual scale data that meets the requirements of the synthesis dataset.

Table 3 Gauge data sources used in this analysis. N1 and N2 refers to numbers of gauges with observations after 1979 and used in GSHA. The starting and ending years (Y1 and Y2) of GSHA gauges for each agency are listed.

Source	N1	N2	Y1	Y2	URL/Provider
ArcticNET 2022	116	106	1979	2003	www.r-arcticnet.sr.unh.edu/v4.0/AllData/index.html
Australian Bureau of Meteorology 2022 (BOM)	4017	2340	1979	2021	www.bom.gov.au/waterdata/
Brazil National Water Agency 2022 (ANA)	1343	1172	1979	2021	www.snirh.gov.br/hidroweb/serieshistoricas
Canada National Water Data Archive 2022 (HYDAT)	3771	2222	1979	2021	www.canada.ca/en/environment-climate-change/services/water-overview/quantity/monitoring/survey/data-products-services/national-
Chile Center for Climate and Resilience Research 2022(CCRR)	481	392	1979	2020	https://explorador.cr2.cl/
Chinese Hydrology Project (CHP)	112	26	1979	1987	(Henck et al 2010, Schmidt et al 2011)
The Global Runoff Data Centre 2022 (GRDC)	6345	4004	1979	2021	(https://portal.grdc.bafg.de/applications/public.html?publicuser=PublicU ser
India Water Resources Information System 2022 (IWRIS)	547	261	1979	2020	https://indiawris.gov.in/wris/#/RiverMonitoring
Japanese Water Information System 2022 (MLIT)	1023	751	1979	2019	www1.river.go.jp/
Spain Annuario de Aforos, 2022 (AFD)	1138	889	1979	2018	http://datos.gob.es/es/catalogo/e00125801-anuario-de-aforos/resource/48368826-e7fd-4a41-950c-89b4eaea0279
Thailand Royal Irrigation Department 2022 (RID)	126	73	1980	1999	http://hydro.iis.u-tokyo.acrpac.jp/GAME-T/GAIN-T/routine/rid-river/disc_d.html
U.S. Geological Survey 2022 (USGS)	16951	9069	1979	2021	https://waterdata.usgs.gov/nwis/rt
Chinese National Real-time Rain and Water Situation Database	527	263	2000	2019	http://xxfb.mwr.cn/sq_zdysq.html

230 ## 3.23 Watershed delineation

231   The watershed delineation process ~~is~~was built upon a vector-based global river network dataset
232 (Lin et al., 2021), which is delineated from the 90-m Multi-Error-Removed Improved Terrain
233 (MERIT) digital elevation model (DEM) (Yamazaki et al., 2017) and the flow direction and flow
234 accumulation rasters (Yamazaki et al., 2019). The locations of the gauges may contain locational
235 errors and direct delineation will result into erroneous watershed boundaries; therefore, gauge
236 location correction was conducted by relocating the gauges to the nearest MERIT-based river reach
237 vertices. The adjusted gauge points ~~are~~were used as the watershed outlets, where the contributing
238 areas ~~are~~were extracted by dissolving all upstream catchments based on the topology provided by
239 MERIT Basins (Lin et al., 2019). Since the area threshold of MERIT Basins is 25 km^2, we ~~do~~did
240 not include watersheds smaller than this threshold. Considering the spatial heterogeneity of very
241 large basins, we excluded watersheds ≥50,000 km^2 from the dataset. To ensure GSHA ~~to~~
242 ~~support~~supports studies with sufficiently long records, only watersheds with >5 years of
243 observations since 1979 were selected. For gauges sharing the same watershed, the one with better
244 data quality (i.e., longer measurement records and more valid observation days) ~~is~~was used. If the
245 two gauges share the same quality, we only included the furthest downstream gauge. Eventually, the
246 selection processes resulted in 21568 valid watersheds out of 35970 gauges initially scraped from
247 the web plus 527 gauges from the Chinese National Real-time Rain and Water Situation Database
248 (**Figure 2**).
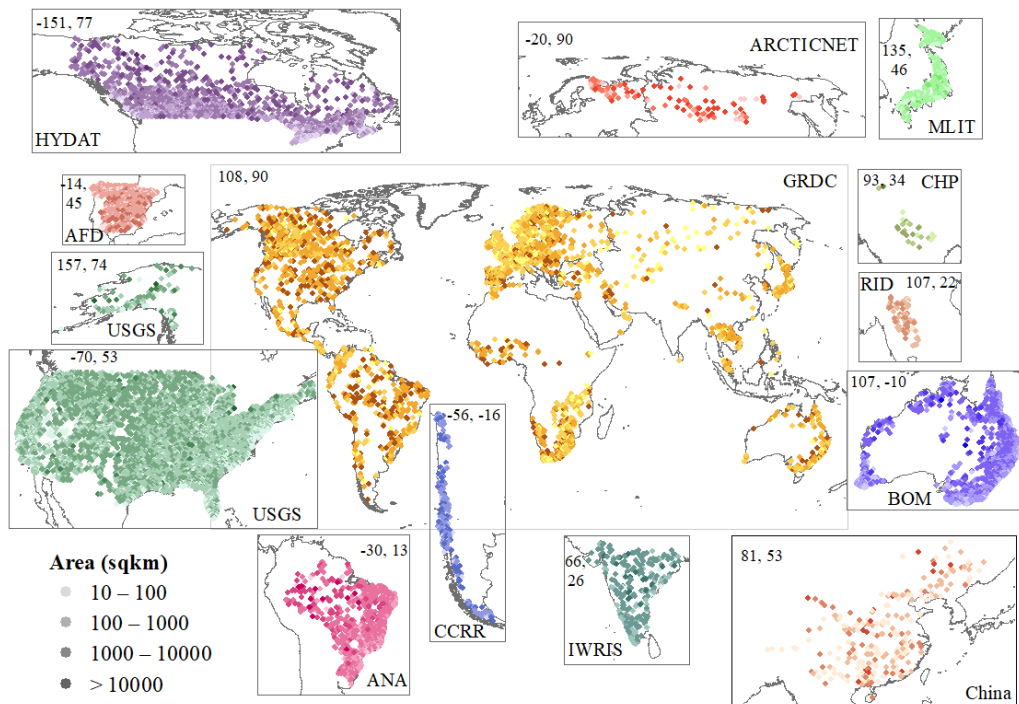
249
250 **Figure 2 Spatial distribution of the GSHA gauges (n=21568).** Watershed areas are represented by the
251 tint of colours. Gauges of different agencies are represented with separate colours and are plotted in
252 individual frames (except for USGS gauges in two frames to incorporate Alaska). The agency names and
253 the upper-left coordinates (longitude, latitude) of each frame are also shown in the figure.
254
255   The GSHA watersheds are unevenly distributed across the globe, more than half of which are

located in North America (USGS, HYDAT, and a large proportion of GRDC gauges, **Figure 3a**). Europe, Australia, and South America also have ~~a~~ relatively good coverage, while Asia and Africa show the lowest gauge densities. The majority of the gauged watersheds are of medium sizes ranging from 250 to 2500 km^2, although for some agencies it does not show the same distribution (**Figure 3d**). For instance, ANA (South America), IWRIS (India~~)~~)), and arcticnet (Northern Eurasia) watersheds are generally larger, while the Chinese National Real-time Rain and Water Situation Database provides more gauges with smaller drainage areas. Due to the maintenance difficulties, the ~~numbers~~number of functioning gauges ~~are~~is declining for agencies like GRDC, but the lack of data in recent years (**Figure 3c**) ~~are~~is mainly due to latency issues. USGS, BOM, and ANA provide a stable number of observations for the 1980-2021 period (**Figure 3c**) with high proportions of valid observations each year (**Figure 3b**), while observational periods from arcticnet and China contain relatively fewer valid samples (**Figure 3b**) and shorter time spans (**Figure 3c**).
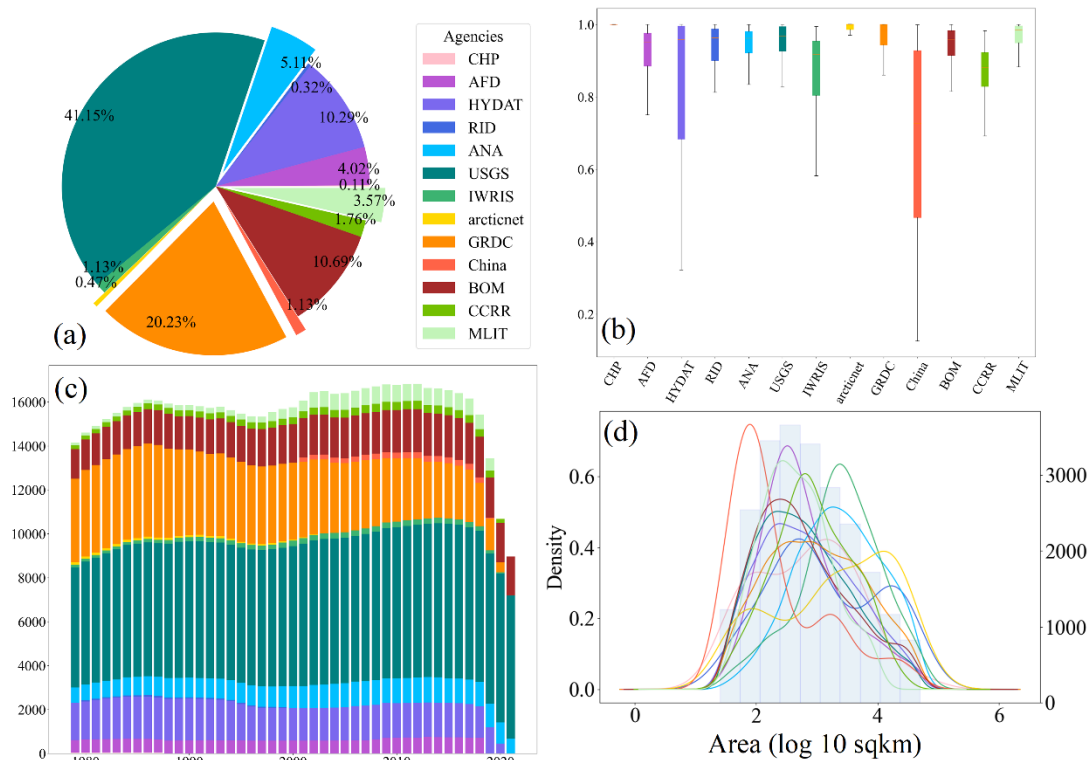
Figure 3 Summary statistics of the GSHA gauges. This includes (a) proportions of gauges from different agencies, (b) box plots for proportions of valid observations for each agency, (c) proportion of valid observation for each year by agency and (d) distributions of watershed areas for each agency (kernel density estimation lines, left y-axis) and all gauges (blue histogram, right y-axis). The colour legend in subplot (a) applies to all four subplots. In subfigure (a) the 0.11% label corresponds to CHP, and the legend goes counter clockwise in the pie chart. In subfigure (c), CHP bars are at the bottom of the plot, and the legend goes from bottom to the top of the bars.

3.~~3~~4 Meteorological variables, water storage terms, and land surface characteristics

After watershed delineation, publicly available grid or non-grid data were obtained and overlaid to derive the meteorological, water storage terms, and land surface characteristics. The data

279 sources used for GSHA are listed in **Table 4**. We prioritized the use of multi-source fusion datasets
280 with relatively high quality surveyed from literature when creating GSHA.

281 3.~~3~~4.1 Meteorology datasets

282 For precipitation, the Multi-Source Weighted-Ensemble Precipitation (MSWEP) that ~~have~~
283 merged gauge measurements (CPC Unified), grid data (GPCC), satellite products (CMORPH,
284 GSMaP-MVK, and TMPA 3B42RT), and reanalysis data (ERA-Interim and JRA-55) with sample
285 density and comparative performance considered (Beck et al., 2017; Beck et al., 2019) ~~is used~~are
286 included. Another ~~recent~~ precipitation dataset is the Ensemble Meteorological Dataset for Planet
287 Earth (EM-Earth) deterministic estimates, which ~~merges~~merged a station-based Serially Complete
288 Earth (SC-Earth) removing the temporal discontinuities in raw station observations and ERA5
289 estimates (Tang et al., 2022). ~~The~~
290 For 2-m air temperature, the EUSTACE global land station daily air temperature dataset
291 (EUSTACE) statistically merged station and satellite observations to obtain global daily near-
292 surface air temperature (Brugnara et al., 2019~~), and is used as a source for 2-m temperature in~~
293 ~~GSHA.~~) is included. Other datasets used for 2-m temperature extraction are the reanalysis datasets
294 Modern-Era Retrospective analysis for Research and Applications Version 2 (MERRA-2) (Gelaro
295 et al., 2017) ~~by NASA's Global Modelling and Assimilation Office (GMAO)~~ and the ~~land~~
296 ~~components of the European Centre for Medium-Range Weather Forecasts (ECMWF)~~ fifth
297 generation of European Reanalysis (ERA5) dataset land component (Muñoz-Sabater et al., 2021).
298 ~~These reanalysis datasets are also used in extracting long- and shortwave radiation, as well as u- and~~
299 ~~v-components of wind.~~ MERRA-2 ~~uses~~, produced by NASA's Global Modelling and Assimilation
300 Office (GMAO), used the Goddard Earth Observing System (GEOS) model and analysis scheme~~,~~
301 and assimilated the latest observations. ~~The land surface model used in~~ ERA5 reanalysis ~~is~~was
302 developed by the European Centre for Medium-Range Weather Forecasts (ECMWF) using the
303 Carbon Hydrology-Tiled ECMWF Scheme for Surface Exchanges over Land (CHTESSEL) driven
304 by the downscaled meteorological forcing from the ERA5 climate reanalysis (Hersbach et al., 2020).
305 These reanalysis datasets are also used in extracting long- and shortwave radiation, as well as u- and
306 v-components of wind.
307 For AET, the REA dataset ~~merging,~~ which used the reliability ensemble averaging (REA)
308 method to merge ERA5, Global Land Data Assimilation System Version 2 (GLDAS2), and
309 MERRA-2 ~~using the reliability ensemble averaging (REA) method~~ is used (Lu et al., 2021~~), together~~
310 ~~with~~). Another AET data source is the product of the Global Land Evaporation Amsterdam Model
311 (GLEAM) based on satellite observations of surface net radiation and near-surface air temperature
312 (Martens et al., 2017). For PET, GLEAM is also incorporated. Another PET dataset for GSHA is
313 ~~the~~an hourly PET at 0.1° resolution for the global land surface ~~from 1981-present~~ (hPET) ~~dataset~~
314 calculated from ERA5-land wind speed, air and dew point temperature, net radiation components,
315 and surface air pressure (Singer et al., 2021).

316 3.~~3~~4.2 Water storage term datasets

317 ERA5-land data ~~was~~is also applied in extracting soil moisture for 4 soil layers, as well as snow

318   water equivalence. For groundwater, an assimilation dataset from ~~the~~ NASA's Gravity Recovery
319   and Climate Experiment (GRACE) and its follow-on mission (GRACE-FO) is used (Li et al., 2019).
320   The dataset merged water storage derived from GRACE satellite products into ECMWF Integrated
321   Forecasting System meteorological data-forced NASA's Catchment land surface model (CLSM).
322   The data is represented as groundwater drought indicator (GWI), which is the percentage of
323   groundwater storage estimates from the GRACE data assimilation relative to the climatology
324   (representing historical conditions), at weekly time scales from 2003-2021.

325   3.~~3~~4.3 Land surface characteristic datasets

326   Global urban development for 1985-2015 is represented as the urban fraction in each watershed
327   using the global annual urban dynamics (GAUD) at 30-m resolution. The dataset was derived from
328   Landsat surface reflectance based on the Normalized Urban Areas Composite Index (NUACI) (Liu
329   et al., 2020). For forest and cropland fractions, the Terra and Aqua combined Moderate Resolution
330   Imaging Spectroradiometer (MODIS) Land Cover Type (MCD12Q1) land cover dataset, ~~was~~is used
331   (Friedl et al., 2010). It covers 2001-2020 with a resolution of 500 m, and the categories used for
332   GSHA ~~is~~are the International Geosphere–Biosphere Programme classification (IGBP) forests and
333   croplands. Another land cover is vegetation, which is represented by LAI obtained from the National
334   Oceanic and Atmospheric Administration (NOAA) Climate Data Record (CDR) of Advanced Very
335   High-Resolution Radiometer (AVHRR) product, which ~~relies~~relied on artificial neural networks and
336   AVH09C1 surface reflectance product (Claverie et al., 2016).

337   3.~~3~~4.4 Dams and reservoirs

338   The newly published Georeferenced global Dams And Reservoirs (GeoDAR) dataset that
339   ~~documents~~documented the dam and reservoir construction years is used for building the temporally
340   varying watershed reservoir capacity and DOR. GeoDAR georeferenced the International
341   Commission on Large Dams (ICOLD) World Register of Dams (WRD), and geo-matched multi-
342   source regional registers and geocoding descriptive attributes through the Google Maps API (Wang
343   et al., 2022). The reservoir capacities are used together with the mean annual streamflow to obtain
344   the DOR based on ~~the~~ equation $dor = SC/Q_{mean}$, where SC refers to reservoir storage capacity
345   and Q_{mean} is the mean annual streamflow in the corresponding year.

346   3.~~3~~4.5 Static variables

347   We matched GSHA river IDs and HydroATLAS river reach IDs to link the static attributes.
348   HydroATLAS includes 56 variables for hydrology, physiography, climate, land cover & use, soils
349   & geology, and anthropogenic influences for over 8.5 million river reaches globally.
350
351   **Table 4 Data sources used for the GSHA variables.**

Category	Dataset	Resolution	Interval	Reference
Meteorology	MSWEP	0.25°	Daily	(Beck et al., 2017; Beck et al., 2019)

	EM-Earth	0.1°	Daily	(Tang et al., 2022)
	ERA5-land	0.1°	Hourly	(Muñoz-Sabater, 2019)
	MERRA-2	0.5°* 0.625°	Hourly	(GMAO, 2015)
	EUSTACE	0.25°	Daily	(Brugnara et al., 2019)
	REA	0.25°	Daily	(Lu et al., 2021)
	GLEAM	0.25°	Daily	(Martens et al., 2017; Miralles et al., 2011)
	hPET	0.1°	Daily	(Singer et al., 2021)
Water storage terms	ERA5-land	0.1°	Hourly	(Muñoz-Sabater, 2019)
	GRACE-FO data assimilation	0.25°	Weekly	(Li et al., 2019; Zaitchik et al., 2008)
Land surface	GAUD	30 m	Yearly	(Huang, 2020)
	MCD12Q1	500 m	Yearly	(Friedl et al., 2019)
	CDR Leaf Area Index	0.05°	Daily	(Vermote et al., 2019)
Dam and reservoir	GeoDAR	NaN (polygon)	Yearly	(Wang et al., 2022)
Static Attributes	HydroATLAS	NaN (line)	NaN (static)	(Lehner et al., 2022; Linke et al., 2019)

3.45 Variable extraction methods

For grid data with relatively coarse spatial resolutions (≥0.05°), we used an area-weighted approach to ~~calculate the weighted average~~extract the variable (Addor et al., 2017) based on the proportion of the ~~variable~~grid area contained in the basin boundary, while for high-resolution grid data, we ~~extract~~extracted the arithmetic mean directly. **Figure 4** shows the area-weighted average approach we used for grid data with spatial resolution ≥0.05° to reduce the influence of watershed area on data uncertainty (Tang et al., 2022). The grid data (**4a**) and the quality-controlled watersheds (**4b**) ~~are~~were overlayed and all grids intersecting with the watershed ~~are~~were obtained (**4c**). For each intersected grid, the proportion of the polygon in the grid ~~is~~was calculated as the weight (dark blue, **4d**); the product of the weight and the corresponding grid value ~~is~~was calculated over all intersected grids (**4e**) and ~~are~~were summed up as the weighted average (**4f**). For wind, the u- and v-wind components ~~are~~were first used to calculate wind speed, then the basin average ~~is~~was calculated with the weighted average approach. For grid data with a spatial resolution of <0.05°, the area-weighted approach ~~is~~was not adopted as it offers limited gains while becoming computationally too expensive. For reservoirs, ~~they are~~we used the reservoir polygons in GeoDAR, which were spatially joined to GSHA watershed polygons~~, and all~~. All the intersected reservoirs were considered contributory to the management of the corresponding watershed and were used to calculate the total reservoir storage capacity and degree of regulation.
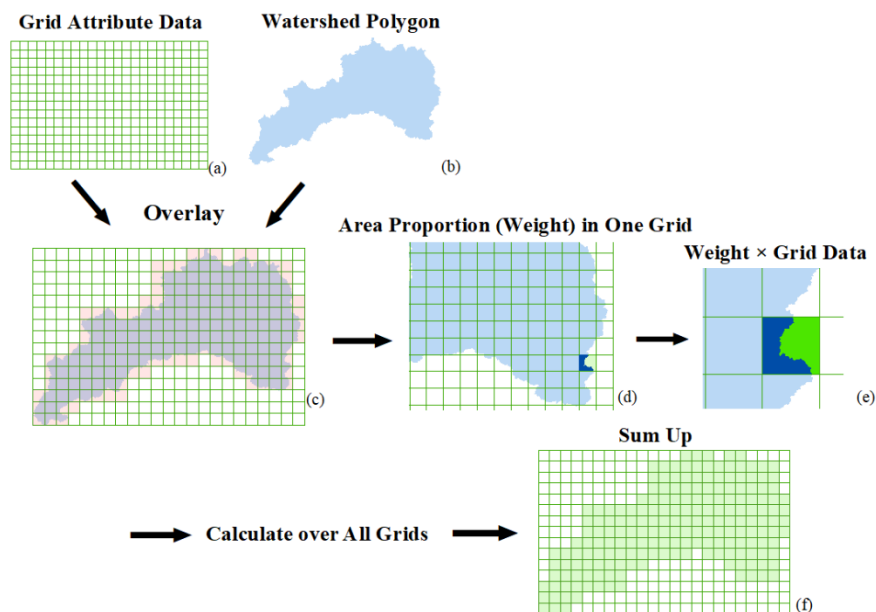
Figure 4 Determination of the area weights in extracting gridded data to GSHA watershed polygons. This weighted approach is applied to data at a resolution of ≥0.05° but not for data at a finer spatial resolution due to computational costs.

3.~~5~~6 Uncertainty estimates

~~For meteorological variables, uncertainty estimates are calculated using Eq. (1):~~

We also provided uncertainty estimates of the meteorological variables by calculating the long-term mean of each dataset in each watershed, where the discrepancy between the maximum and minimum among the data sources (X_{max} and X_{min}) as a percentage of their mean ($\bar{X}$) was used in the uncertainty estimation (see Eq. 1):

$$uncertainty = \frac{X_{max} - X_{min}}{\bar{X}} * 100\%, \tag{1}$$

~~where X_{max} and X_{min} are the maximum and minimum among the extracted values from the independent data sources. $\bar{X}$ is the mean of values from all datasets. The uncertainty ranges from 0 to 200%. Note that for some of our data sources such as EC-Earth, uncertainty estimates are intrinsically provided, but here we do not include it into GSHA as we consider the uncertainty estimates made from independent data sources more internally consistent among different variables.~~

~~3.6 Validation~~

3.7 Validation

After delineation, we validated our watershed areas with officially reported watershed areas from BOM, HYDAT, and GRDC by matching GSHA watersheds by their agency IDs. We set the

criteria of mismatched watersheds as (1) the area difference being over ±20% of the officially reported area, and (2) the area ratio being less than 0.1 or over 10 times the reported areas. Since not all agency websites reported watershed areas, thus we added a flag field in the attributes as "unverified", "verified match", and "verified mismatch" to allow users to filter the watersheds flexibly and avoid putting the samples in the dataset under an unfair standard.

Postprocessing of the extracted variables ~~include~~includes the unification of units and manual quality checks. For streamflow characteristics, we validated three of our indices against GSIM for its global coverage, including the mean annual streamflow, ~~10^{-th}~~10th and ~~90^{-th}~~90th percentiles. The spatial joint between GSHA and GSIM gauges in a 10 km buffer zone was performed, and only the GSIM gauge with a minimum distance and watershed area difference ≤5% to a GSHA gauge ~~is~~was considered. Pairs with 0 measurements were excluded and 9835 pairs were involved eventually. We plotted the scatter plot of GSHA-GSIM mean flow, 10^{-th} and 90^{-th} percentiles, and compared the fitting line to the 1:1 line, with correlation coefficients calculated (see Section 4.1).

We also validated precipitation, potential ET, and 2 m air temperature with the regional CAMELS-US dataset. We ~~compare~~compared the Daymet meteorological variables of CAMELS and the mean of GSHA variables for ~~the~~validation. Since we ~~include~~included ERA5 data for most of our variables directly or indirectly as the data source, while Caravan consistently used ERA5, we did not use Caravan for the global validation as it is not considered as fully independent from GSHA. The spatial match ~~is~~was the same as we did for GSIM which resulted in 906 pairs. This number ~~is~~was larger than the total CAMELS gauge numbers as some gauges might be repeatedly paired due to location bias of the USGS gauges and MERIT river networks, as well as the adjacency between gauges of different agencies. Similarly, scatter plots and correlation coefficients are provided for assessment.

3.~~7~~8 Watershed classification and change detection

We classified the watersheds as natural and human-managed to analyse the influence of human water management. A watershed is classified as a natural watershed if it satisfies the following: (1) DOR is smaller than 10%; (2) the urban extent is less than 5%; and (3) the sum of urban and cropland fractions is smaller than 10% (L. Yang et al., 2021; Zhang et al., 2023). The classification was performed for 2001-2015, and the changing patterns of the watersheds are divided into six categories: (1) natural (N) when the watershed remained natural for all 15 years; (2) human managed (H) when the watershed remained human managed for all 15 years; (3) natural to human managed (NH) when the watershed was first natural in 2001, but changed to and maintained human managed later; and (4) human managed to natural (HN) when the watershed was first human managed in 2001, but changed to and maintained natural later.

4 Results

As previous studies have already revealed the spatial patterns of the LSH hydrometeorological variables both locally and globally, ~~therefore~~here we put the spatial patterns of GSHA

428 meteorological variables and streamflow indices in **Appendix A**, while we focus on using the

429 Results section to reveal the uniqueness of GSHA~~, which includes~~. These include a technical

430 validation of GSHA, uncertainty analysis, and the temporal change of watershed human

431 management levels.

4.1 Technical validation

433 The validation result figures of watershed areas are in **Appendix B** since we focused more on

434 the variables and already added the validity results in the dataset as "unverified", "verified match",

435 and "verified mismatch" fields in the dataset. Under our criterion of filtering "mismatch" watersheds,

436 1.9% of BOM watersheds, 4.7% of HYDAT watersheds and 8.9% of GRDC watersheds are

437 mismatched. After removing these watersheds, correlation coefficients between GSHA and the

438 agencies can reach 0.99, which verified the correctness of our watershed delineation and data

439 extraction approach.

440 **Figure 5** illustrates the validation results of GSHA. **Figures 5a–5c** show streamflow indices

441 as validated against GSIM globally, and **Figures 5d–5f** show meteorological ~~variable~~variables as

442 validated against Daymet from CONUS CAMELS. For streamflow indices, precipitation, and

443 temperature, the correlation coefficients exceed 0.95 (significance p<0.01), and the fitting lines are

444 close to the 1:1 line, indicating high consistencies between GSHA and the reference datasets. For

445 PET, however, the coefficient is low, at only 0.573 (significance p<0.05), and the CAMELS PET is

446 generally higher than GSHA ensemble, which is possibly ascribed to the high uncertainty among

447 PET datasets that is yet to be fully resolved (Singer et al., 2021) (see **Appendix** ~~B).~~ C). Note that

448 the gauge pairing might bring a small proportion of wrong pairs for some very close gauges, and

449 differences in temporal ranges of GSHA and GSIM might cause some discrepancies for observed

450 streamflow.

451
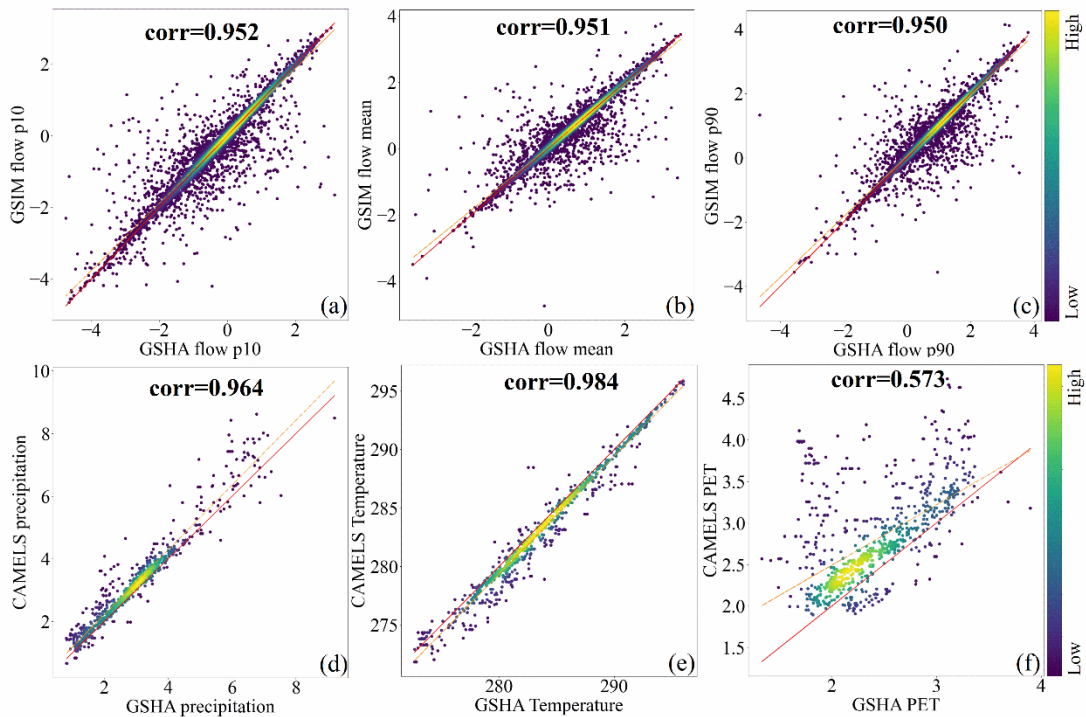
452 **Figure 5 Validation of GSHA with GSIM streamflow characteristics ((a), (b) and (c)), and**

453 **CAMELS meteorological variables ((d), (e) and (f)).** 'Corr' in the subfigure is the Pearson correlation

454 coefficient. The red line is the 1:1 line, while the orange dotted line is the fitting line of the scatter points.

455 The colour bar represents density of the sample points. The unit of X and Y axes in (a), (b). and (c) is

456 long10 m³/s.

4.2 Uncertainty patterns for the GSHA meteorological variables

458 **Figure 6** shows the distributions of the uncertainties for different variables, and the colour bars

459 are unified to allow for comparisons between different variables.
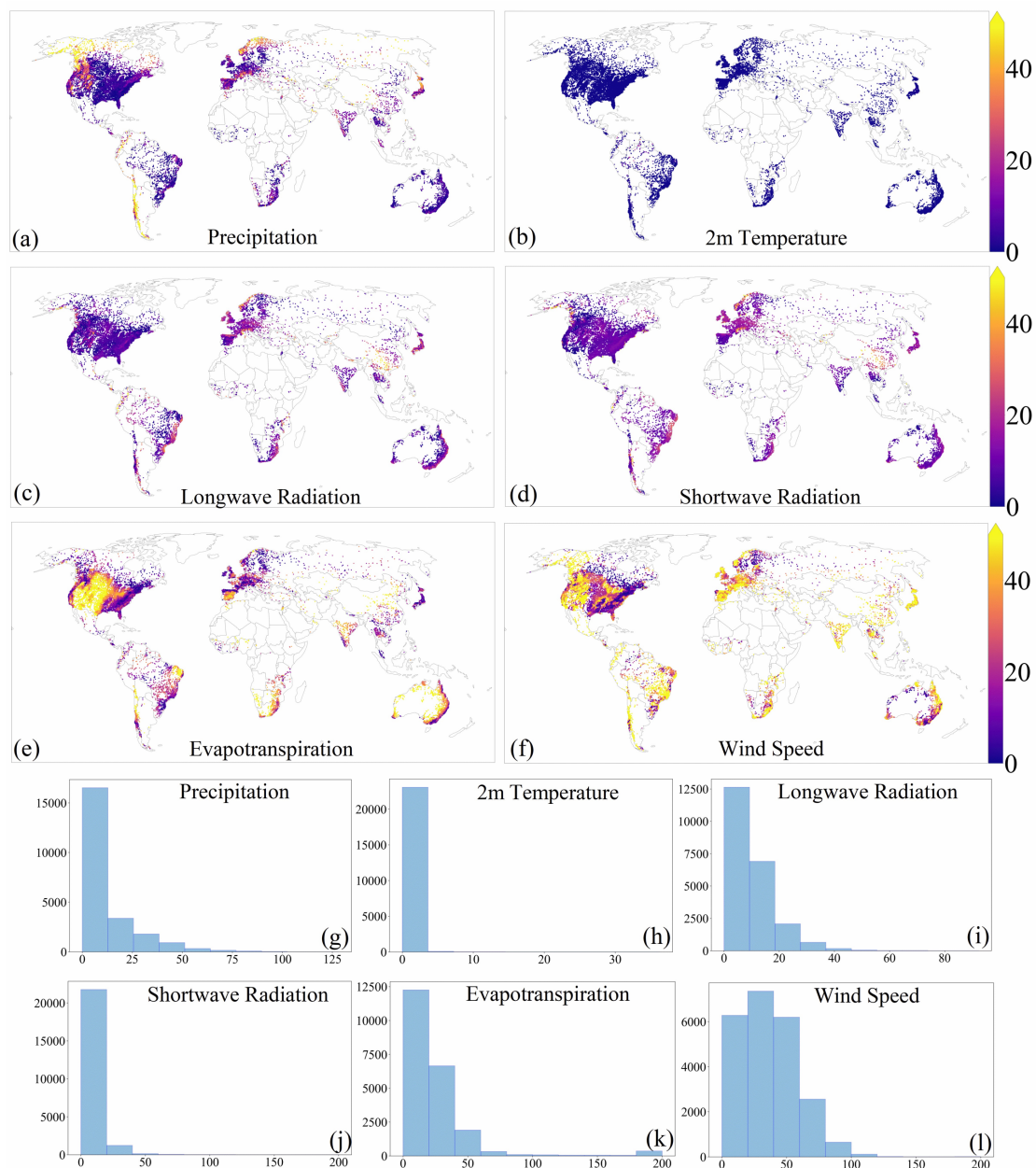
461 **Figure 6 Global patterns of the uncertainty for the GSHA meteorological variables (in percentage).**

462 This includes the uncertainty (a) for precipitation (mm/day), (b) 2-m temperature (K), (c) longwave

463 radiation (W/m²), (d) shortwave radiation (W/m²), (e) evapotranspiration (mm/day), and (f) wind speed

464 (m/s), and (g) the uncertainty histogram for precipitation, (h) 2-m temperature, (i) longwave radiation,

465   (j) shortwave radiation, (k) evapotranspiration, and (l) wind speed.

466

467   Generally, among all variables, air temperature (**Figures 6b & 6h**) shows the minimum

468   uncertainty (<5%), ~~while the~~suggesting high consistency of air temperature estimates from different

469   datasets. The uncertainty for wind speed (**Figure 6f**) is the highest among all variables. Uncertainties

470   for other variables show strong spatial variability. For example, uncertainties for precipitation are

471   high in high-latitude or mountainous areas like the Rocky Mountains, northern Europe, the Alps,

472   and the Andes areas (**Figure 6a**). This is reasonable because limited accessibility to in-situ

473   observations and the misestimation of snow (Schreiner-McGraw & Ajami, 2020) can contribute to

474   ~~the~~ precipitation estimation errors, while the data sources show relatively high consistency

475   (*uncertainty* ≤25%) in other parts of the world (**Figure 6g**). For radiation, as solar/shortwave

476   radiation is largely affected by sky conditions, ~~thus~~ uncertainties are high in regions with less clear

477   sky, including south-west China and its surrounding areas, high latitude regions of the northern

478   hemisphere, and Europe (Brun et al., 2022). These places are also subject to high thermal/longwave

479   radiation uncertainties for similar reasons (**Figure 6c**). Land cover including vegetation and

480   artificial surface, is another factor influencing surface net radiation through the albedo effect (Hu et

481   al., 2017), thus for heavily vegetated and urbanized areas, such as the Amazon region and east

482   coastal Australia, uncertainties for both longwave and shortwave fluxes are also relatively high.

483   Nevertheless, **Figures 6i & 6j** demonstrate that for the majority of watersheds, radiation

484   uncertainties are < 25%, indicating that the radiation data sources are generally consistent ~~to~~with

485   each other. ET uncertainties are generally larger than the above variables (**Figures 6e & 6k**), and

486   are particularly prominent in dry areas of the globe, e.g., central North America, northern Andes,

487   central Asia, and Australia's grasslands and deserts. It is also prominent in agriculture intensive

488   regions like India and the northern part of China (Sörensson & Ruscica, 2018), where ~~the~~

489   agricultural irrigation may be the contributing factor to the ET uncertainty. The spatial distributions

490   of wind speed do not seem to show clear regional patterns (**Figure 6f**), and uncertainty values of

491   wind speed are generally larger over the majority of watersheds (**Figure 6l**). Nevertheless, the

492   uncertainties are low in ~~the~~ Appalachia and northern Europe, and are high in most parts of Brazil,

493   the Andes, Africa, eastern and southern parts of Asia, as well as Australia (**Figure 6f**). As we already

494   selected relatively high-quality datasets for the variables, these areas might be calling for more

495   attention by the LSH developers, while providing possible explanations for the inconsistencies in

496   interpreting results or understanding the challenges in estimating model parameters by the LSH

497   users.

498
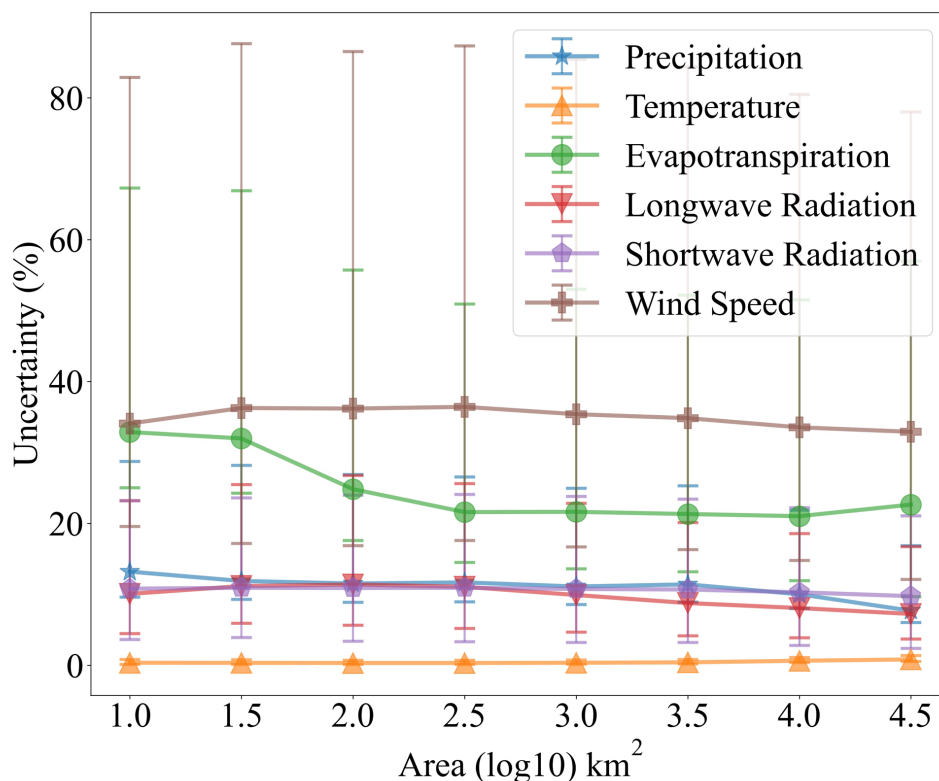
Figure 7 Relationship between variable uncertainties and watershed areas. The markers indicate mean values of the variable uncertainties in watersheds smaller than the corresponding x-axis value. The error bars represent the range between 25 and 75 percentiles of the uncertainty values.

Apart from the spatial ~~characteristics~~patterns above, we also ~~investigate~~investigated the emergent patterns of the uncertainties. Existing studies indicate small basins can show larger uncertainties due to coarse resolution data inputs (Kauffeldt et al., 2013), while sub-grid variabilities might be offset by averaging over large watersheds. ~~Therefore,~~As we plotted the uncertainty against watershed areas in **Figure 7**, ~~which~~it verifies that for most variables, the uncertainty declines as the watershed area increases. ~~In addition to the general understanding,~~ **Figure 7** also reveals some interesting patterns.~~ The ~~ which were rarely discussed in existing studies. For example, the most obvious decline ~~comes~~of data uncertainty with area came from ET (green~~) and longwave radiation (red), both of which are~~). ET is highly dependent on ~~the land surface conditions and are~~and significantly affected by land surface spatial heterogeneity, thus ~~benefiting~~it benefits the most from spatial averaging for large river basins. Longwave radiation uncertainty (red) experiences a moderate decline, likely due to its linkage with land surface complexity and cloud conditions. Shortwave radiation and precipitation uncertainty show a similar decline pattern (blue and purple), which is possibly related to their strong ties to cloud covers. Temperature has a low uncertainty, and its relationship to watershed area is also not obvious. Wind speed uncertainty only declines slightly as the area increases, and ~~we believe~~ this ~~is~~may be because wind speed uncertainty can be traced back more to the atmospheric circulation patterns instead of ~~the~~ land surface conditions, thus showing a non-prominent relationship with watershed area. Overall, GSHA provides uncertainty estimates that capture these prominent patterns, which can be helpful to hydrologic modellers and users.

4.3 Natural and human managed watersheds and changing patterns

We also demonstrate the other key features of GSHA by categorizing global watersheds into natural and human--managed, and more prominently their temporal shifts in **Figure 8**. Overall, the majority of human--managed watersheds ~~locates~~are located in the US, Europe, and other regions with intensive industrial or agricultural activities such as East and South Asia (**Figures 8a and 8b**). During 2001-2015, 46.89% of the watersheds remained natural, while another 47.62% under human management in 2001 remained in the category throughout the study period (**Figure 8d**). Generally, the northern hemisphere has a larger proportion of human--managed watersheds, while watersheds in the less populated and urbanized southern hemisphere largely remain natural.

Noticeably, 4.36% of GSHA watersheds switched from natural to human--managed (1011 watersheds), and the remaining 1.13% changed ~~backed~~back to natural states from human managed during 2001-2015. For instance, watersheds in the middle and lower Yangtze River area ~~in~~and the north-eastern China show a shift from human--managed to natural state, where ~~environmental projects for~~ecological restoration projects were in place (Qu et al., 2018; Zhang et al., 2015). Although the time span of GSHA LULC dynamics restricted the change detection for developed ~~regions~~countries as their urbanizations and infrastructure developments have long been completed, and for fast emerging economies after 2015, the time series ~~are~~were also missing; nevertheless, the changing human activities captured by GSHA may be helpful to understand the streamflow changes including flood characteristics (~~Long~~Yang et al., 2021; Zhang et al., 2022).
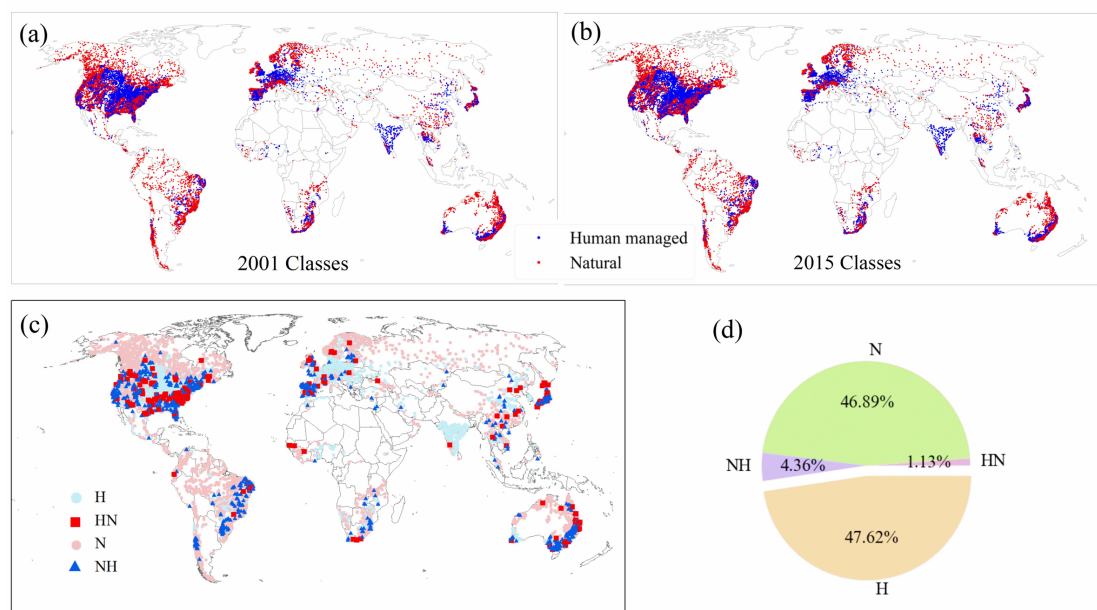
Figure 8 Classification of natural and human managed watersheds in 2001 (a) and 2015 (b). Changes in watershed categories are illustrated by (c) and (d). H and N in (c) and (d) represent watersheds that maintained human managed or natural from 2001-2015; NH and HN represent those changing from natural to human managed and from human managed to natural, respectively.

We further ~~use~~used several examples to illustrate the changing status of GSHA watersheds (**Figure 9**). **Figures 9a and 9b** show a watershed located in ~~Northeastern~~Northeast China, where

550   the rapid increase in cropland shifted the watershed from natural states to human-managed in recent

551   years. **Figures 9c and 9d** correspond to a mountainous area in Sichuan Province, China, which

552   became human-managed due to the construction of a reservoir in 2006. For another case in

553   ~~Northeastern~~Northeast China (**Figures 9e and 9f)** and a USGS case (**Figures 9g and 9h**), the

554   watersheds shifted from human-managed to natural, which is mainly manifested by the reduction

555   in cropland fraction due to the environmental policy. For instance, afforestation during 2000-2010

556   in Changbai Mountains where the watershed in **Figures 9e and 9f** is located, significantly increased

557   the forest cover and might bring a decline in human disturbance in the form of land use (Zhang &

558   Liang, 2014). These results highlight the shifting watershed status that would require further

559   attention from LSH users, which is encapsulated in GSHA v1.0 and will be continuously improved

560   in the future.
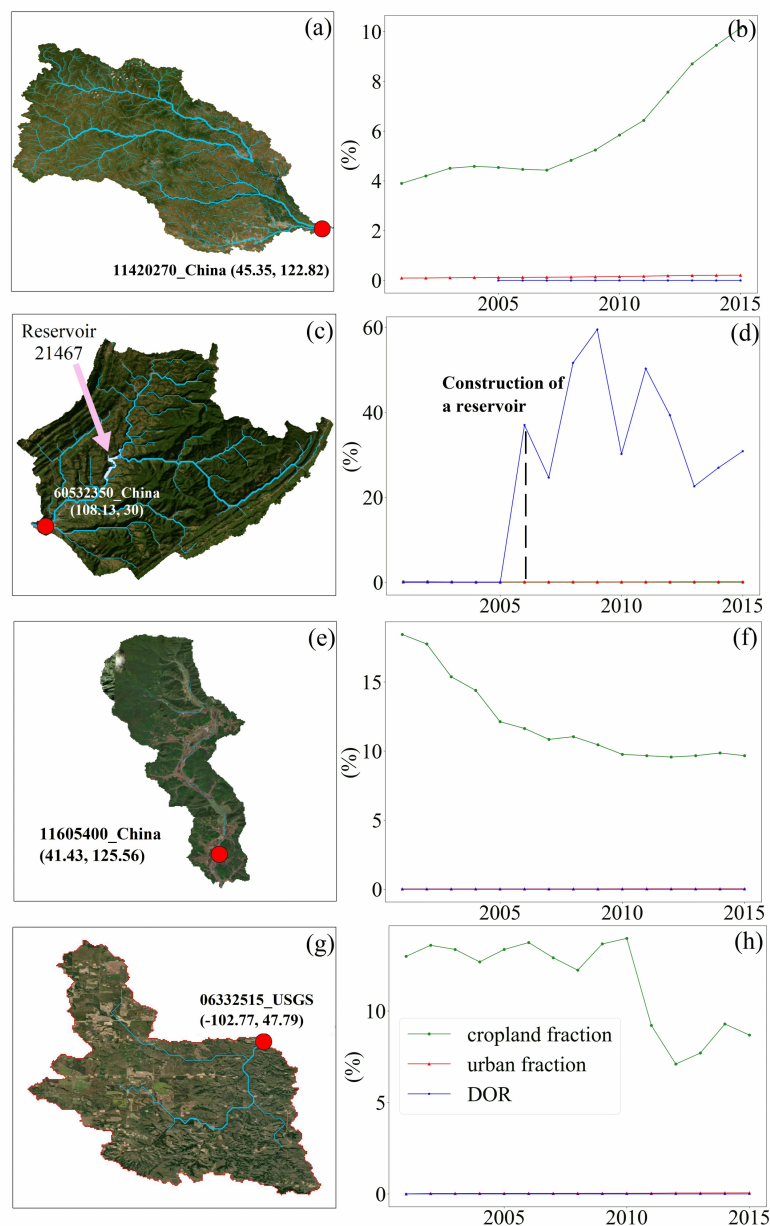
561

562   **Figure 9 Cases for shifting status of the watershed classification.** (a) and (b) correspond to

563   11420270_China, and (c) and (d) correspond to 60532350_China, both of which changed from natural

564   to human managed category. (e) and (f) represent11605400_China, and (g) and (h) correspond to

565   06332515_USGS watershed changing from human managed to natural watershed.

4.4 Changing runoff coefficient patterns derived from GSHA

567   Finally, we also analysed the ~~spatial~~global pattern ~~and~~in the trend of ~~global~~ runoff coefficient

568   (RC~~),~~;) as a brief demonstration ~~of~~on what GSHA can offer out of its many potential usages. RC is

569   defined as R/P, where R denotes runoff (mm) and P denotes precipitation (mm~~) in the~~

570   ~~corresponding period.~~). **Figure 10a** shows that~~,~~ regions ~~where~~with high RC (i.e., a large proportion

571   of rainfall goes into rivers instead of being evaporated or consumed ~~(i.e., high RC~~) are in east Asia

572   and North America, most parts of Europe, the west coast of North America and the Amazon, in

573   general agreement with the aridity patterns across the globe. For arid/semiarid areas and places with

574   intense water use (e.g., western US, eastern Brazil, Australia, Africa), RC is low, meaning most of

575   the precipitation does not reach the gauged river.

576   ~~Interestingly, we show the RC trend for the past decades.~~ We found that RC generally remained

577   stable ~~in most parts of~~for the ~~world~~past decades (i.e., grey dots~~,~~ in **Figure 10b**~~), where~~; >80% of the

578   gauges ~~do~~did not ~~show~~observe a statistically significant trend), while 4252 watersheds observed a

579   statistically significant trend ~~(p>0.05). In total, 4252 watersheds demonstrate a 95% significant~~

580   ~~trend~~ in RC at 95% level (5690 watersheds at ~~a~~ 90% ~~significance~~ level~~), and among~~). Among them,

581   decreasing RC is more widespread ~~compared to~~than increasing RC. The most pronounced ~~RC~~

582   decreasing trends are observed in Europe, India, eastern Brazil, Chile, eastern Australia, and the

583   Euphrates and Tigris, which largely correspond to regions with known ~~increasing~~intense agricultural,

584   industrial, and residential water use that may have reduced the river water. We ~~also found~~note that

585   the global RC trend patterns ~~are~~were different from a recent study ~~showing~~that showed mostly

586   increasing RC in the high-~~latitude watersheds~~latitudes, central North America, eastern Australia,

587   and Europe~~, which can largely be explained by the ET changes~~ (Xiong et al., 2022). ~~Here GSHA~~

588   ~~reveals that RC trend~~Given Xiong et al. (2022) used estimated runoff while we used runoff directly

589   from gauge observations, it is ~~decreasing more widely than the increasing trend, which may be~~likely

590   that the concerning ~~for the~~ water availability issues in the context of increasing human water use

591   may not be fully captured by existing studies. Regional studies also tend to show inconsistent results.

592   For example, a ~~changing~~study based on models incorporating climate~~,~~ change and land use change

593   but ignoring human water consumptions suggested that deforestation and ~~will warrant more future~~

594   ~~research along this line.~~urbanization generally increase RC (Lucas-Borja et al., 2020), while another

595   study identified a significant decreasing trend for RC by focusing on cases with intense irrigational

596   water use (Banasik and Hejduk, 2012). These collectively preclude a clear identification of

597   consistent RC trends (Velpuri and Senay, 2013) and a clear causal factor attribution given the

598   complexity of the anthropogenic factors. As such, GSHA may offer a new path to fill in the gap of

599   disentangling the influences of large-scale water use on decreasing RC.
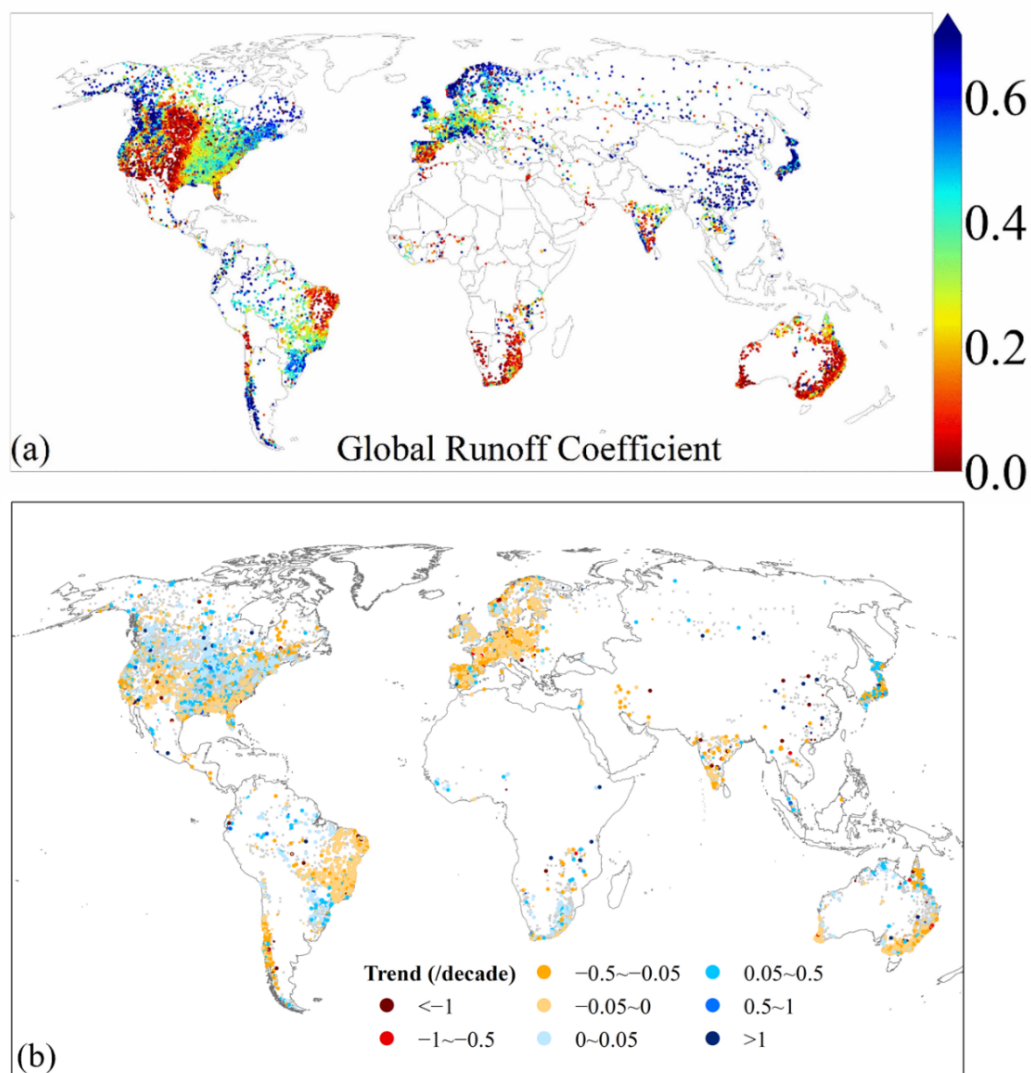
Figure 10 Patterns of runoff coefficient (a) and its trend (b). Only watersheds with statistically significant trend (p<0.05) are shown with colours in (b); the small and large sized points represent 95% (p<0.05) and 90% significance level (p<0.1), respectively. Note that the temporal coverage is different for different gauges; readers can refer to the GSHA temporal coverage for interpreting the patterns. The figure illustrates 18987 GSHA watersheds. Watersheds with less than 10 years of indices calculated from over 250 valid observations per year, as well as with runoff coefficient trend over 20 per decade, are not demonstrated in subfigure b.

5 Conclusions

Large sample hydrology (LSH) datasets play a critical role in data-driven analyses and model parameter estimation for hydrological studies. From MOPEX (Duan et al., 2006) to Caravan (Kratzert et al., 2023), significant efforts have been made to improve the comprehensiveness of LSH, yet issues related to ~~data spatial coverage,~~ uncertainty estimates, and ~~the~~ human activity dynamics ~~and the data spatial coverage~~ remain to be solved. This study ~~focuses on~~

614 ~~complementing~~complements existing LSH with a new synthesis dataset named the Global
615 Streamflow characteristics, Hydrometeorology, and catchment Attributes for large sample river-
616 centric studies (GSHA v1.~~0~~1).

617   To summarize, GSHA contributes the following aspects to the LSH development:

618 1. It includes streamflow indices, hydrometeorological data, and surface characteristics data for
619   21568 gauges compiled from 13 agencies worldwide, which represents one of the most
620   comprehensive LSH by far.

621 2. We ~~incorporate~~incorporated multiple data sources to provide uncertainty estimates for each
622   meteorological variable (including precipitation, 2 m air temperature, radiation, wind, and ET).
623   The spatial patterns and the relationship between the uncertainty and the watershed
624   characteristics ~~that~~ GSHA ~~revealed~~reveals may be helpful to identify inconsistencies among
625   data-driven studies or biases for model parameter estimation studies using existing LSH.

626 3. Dynamic data are provided for previously static data descriptors for land cover changes
627   including urban, cropland and forest fractions, as well as reservoir storage change including
628   storage capacity and degree of regulation.

629   Although GSHA does not cover watersheds of <25km^2 or the dynamics of cryosphere variables
630 (e.g., glacier and permafrost) that have become increasingly important in terrestrial hydrological
631 changes, and the time spans for the dynamic descriptors of LULC are unable to cover the critical
632 periods for the advanced and less-advanced economies due to the constraints with existing LULC
633 data, GSHA is expected to be utilized to unravel the following insights:

634 1. The uncertainty patterns vary between variables and geographical regions, indicating that the
635   interpretation of model and analysis results need to consider inconsistencies of raw data, apart
636   from looking into the methodologies and patterns themselves.

637 2. Although most watersheds have remained natural or human managed throughout the GSHA
638   time span, a considerable number of watersheds shifted between the two categories, which can
639   be ascribed to urbanization, cropland increase, reservoir construction and ecological restoration
640   such as returning farmland to natural states, and these can be clearly manifested using GSHA.

641 3. Analysis with runoff coefficient reveals that ~~while ~80% of~~among gauges ~~do not observe~~with
642   a statistically significant trend, a greater portion ~~of gauges have~~ experienced a declining RC
643   trend than an increase trend. This pattern revealed by GSHA can be used to further study water
644   availability issues in a changing climate.

645   As our knowledge on the above processes continues to improve, we expect that future versions
646 of GSHA will be continuously updated. Finally, better hydrological data sharing is crucial to
647 advance global change hydrology studies.

Appendix

A. Spatial patterns of GSHA meteorological variables

650   **Figures A1 & A2** show the spatial distributions of GSHA meteorological variables and selected

651 streamflow indices. The spatial pattern derived from each individual data source is plotted separately.
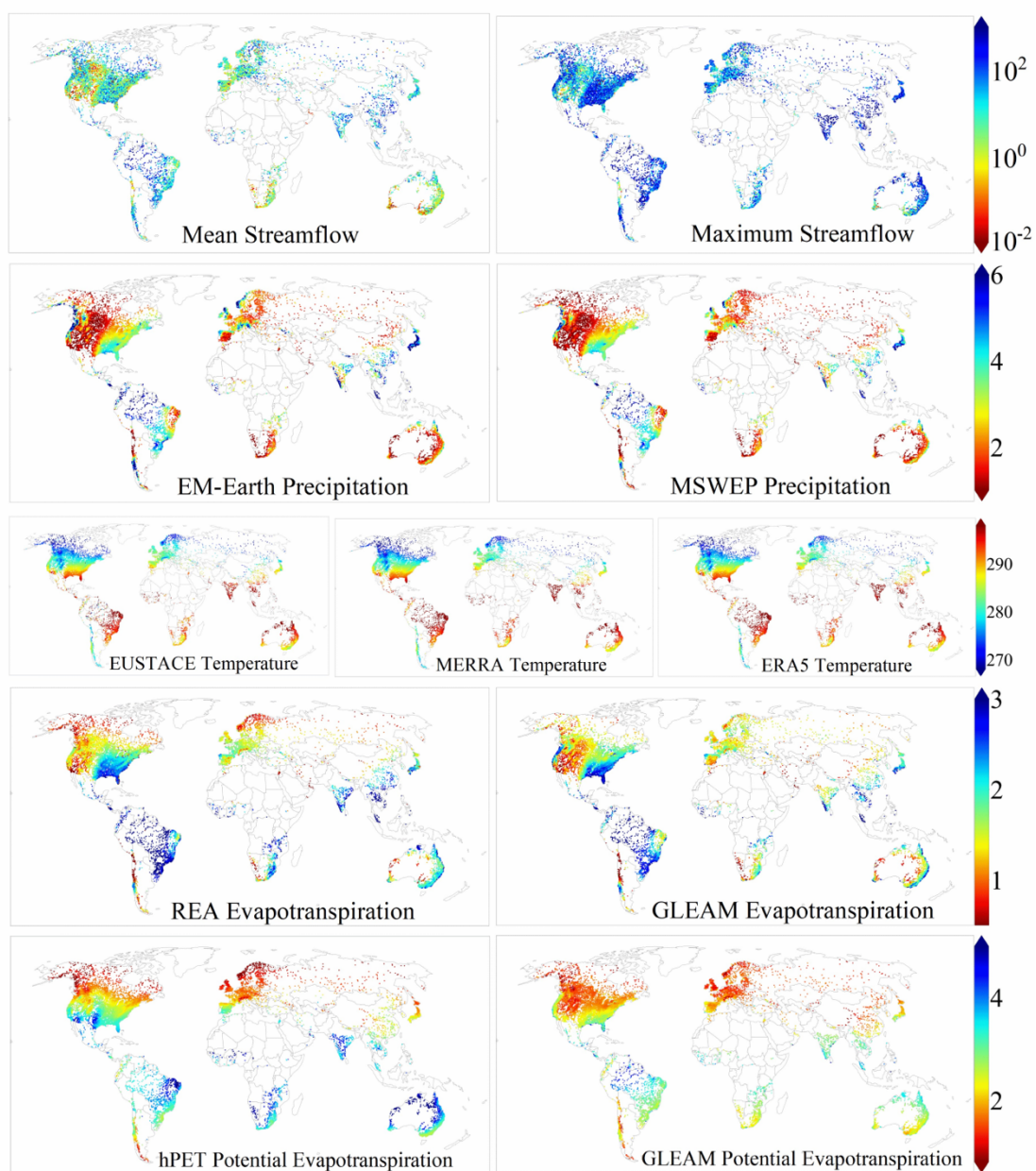
652

653 **Figure A1** Spatial distribution of streamflow indices (row 1, m³/s), precipitation (row 2, mm/day), 2 m

654 air temperature (row 3, K), actual ET (row 4, mm/day), potential ET (row 5, mm/day).
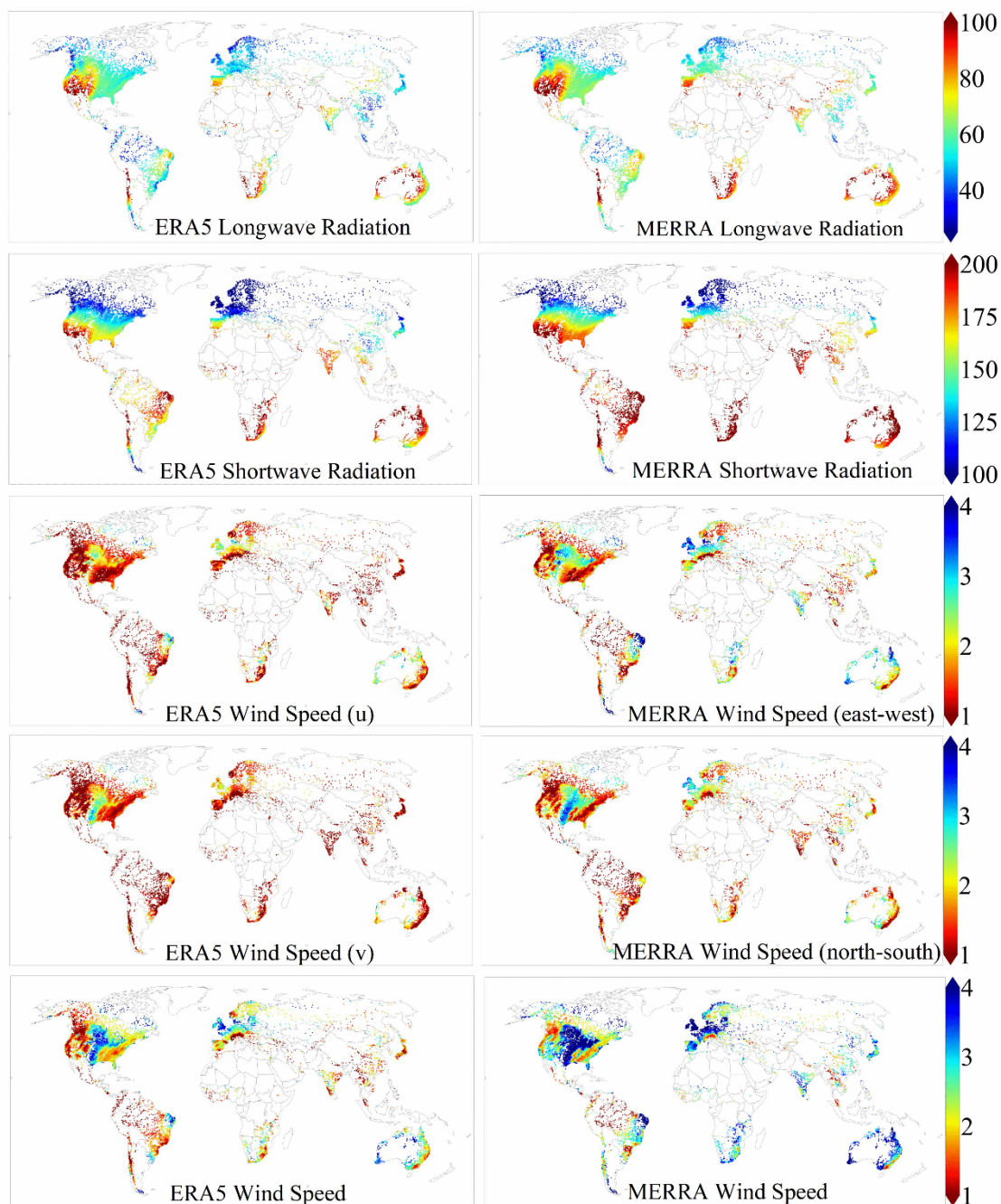
Figure A 2 Spatial distribution of longwave radiation (row 1, W/m^2), shortwave radiation (row 2, W/m^2), wind u- (row 3, m/s) and v- components (row 4, m/s) and the wind speed (row 5, m/s).

B. Validation results of watershed areas

The validation results with BOM, HYDAT, and GRDC on watershed areas are plotted in **Figure B1** and **B2**, where the mismatches between GSHA areas and the officially reported areas are shown. Before removing the mismatched watersheds, their correlation coefficients are 0.960, 0.840, 0.709, respectively, as showm in **Figure B1 (a), (b), (c).** After removing the mismatched watersheds, correlation coefficients for all three agencies reach 0.999, as shown in **Figure B1 (d), (e), (f)**. As we

665 traced the MERIT Basins (Lin et al., 2019) for our watershed delineation, the mismatches are
666 believed to occur when the gauge locates in the vicinity of the intersection point of a river reach and
667 its main stream, which makes it difficult to decide which reach the gauge belongs to while matching
668 the gauge to the MERIT river network. This explains why in **Figure B1** most of the mismatches
669 appear at relatively small areas. As we do not have access to all official watershed areas, and **Figure**
670 **B1 (a), (b), (c)** suggest that matching qualities differ among the agencies, to simply remove the
671 mismatched watersheds or to modify them might put the samples in the dataset under an unfair
672 standard. Additionally, some agencies such as GRDC experienced some updates of their gauige
673 locations and upstream areas, thus watershed boundaries in all datasets mentioned might come with
674 uncertainties. Therefore, we gave the watersheds as "unverified", "verified match", and "verified
675 mismatch" identifiers to allow users to flexibly filter the watersheds.
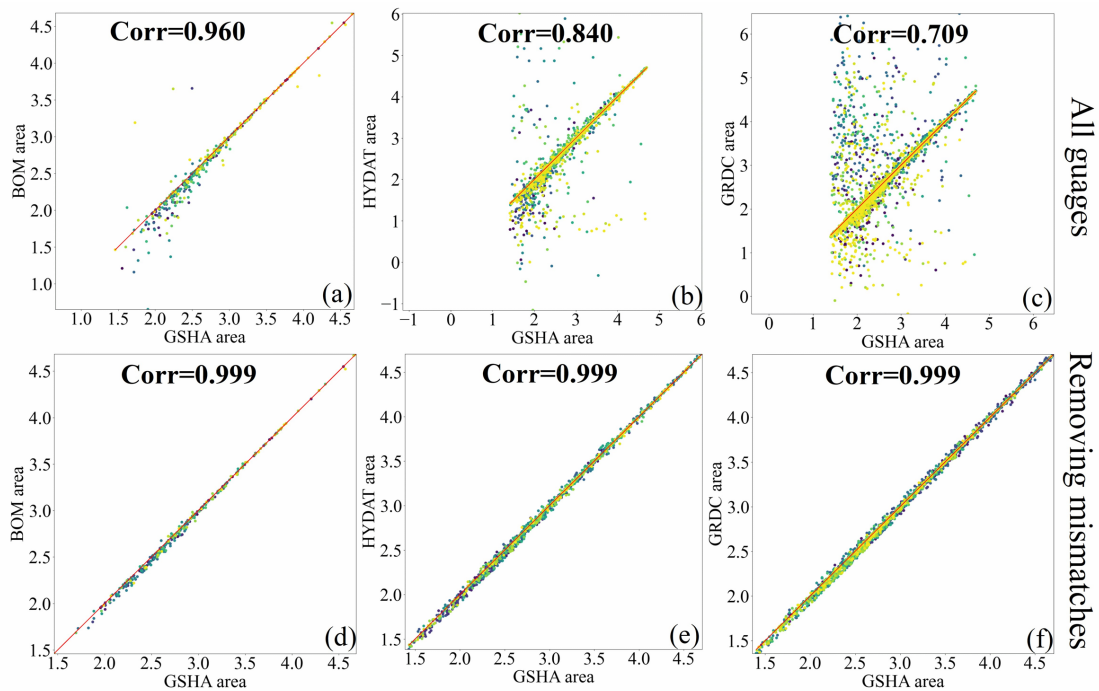
676
677 **Figure B1** Validation of GSHA with officially reported areas of BOM (a, d), HYDAT (b, e), and GRDC
678 (c, f). Subfigures (a) to (c) are the results before removing the mismatched watersheds, and subfigures
679 (d) to (f) represent results after removing the mismatched watersheds. The Pearson correlation coefficient
680 are represented by "Corr" in the figure. The areas are represented by the unit of (log10 km2).

681 ~~B.~~**C.**   **Potential evapotranspiration uncertainty**

682   The spatial and numerical distributions of potential evapotranspiration (PET) uncertainties are
683 illustrated in **Figure ~~B1~~C1** and **Figure ~~B2~~C2**. PET uncertainty is high compared with other
684 variables (see 5.2 section). The majority of high PET uncertainty watersheds are in dry areas, but
685 since it is calculated from meteorological variables, exceptions exist for palces including eastern
686 Pacific coast, where the climate is dry but PET uncertainty is low, and India, which is located in a
687 wet climate zone but has high PET uncertainty. As demonstrated by **Figure ~~B3~~C3**, PET uncertainty
688 do not decrease with the increase of watershed area, probably because PET is calculated from
689 various variables, and the calculation over large watersheds involves more uncertainties for
690 individual grids.
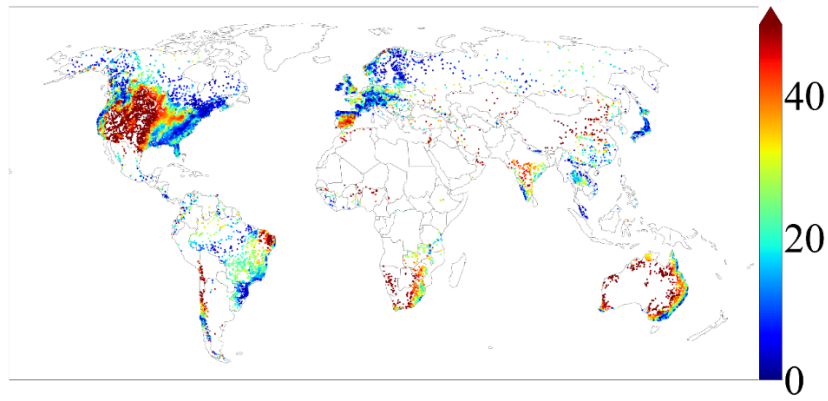
691
692 **Figure B1C1** Spatial pattern of potential evapotranspiration (PET) uncertainty.
693
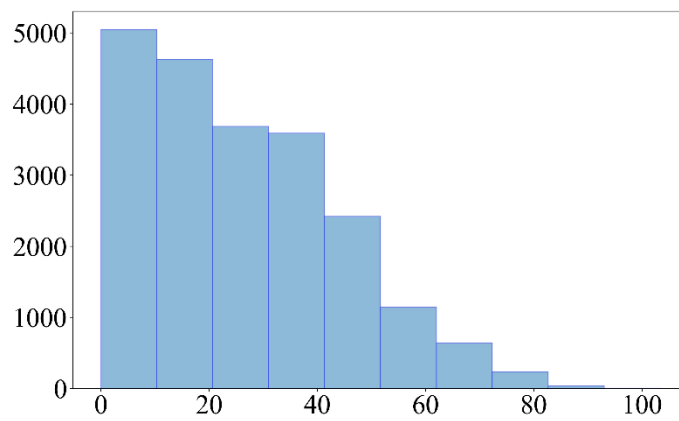
694
695 **Figure B2C2** Numerical distribution of PET uncertainty.
696
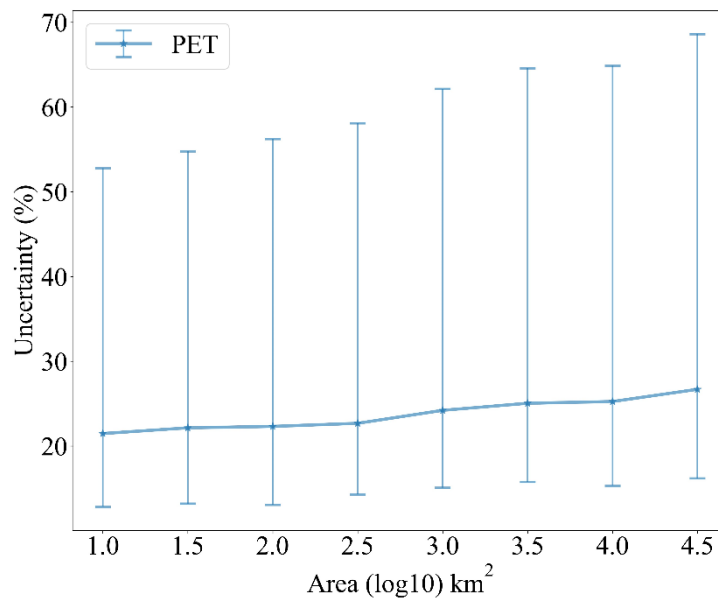
697
698 **Figure B3C3** Relationship of PET uncertainty to watershed area.

Author contribution

Conceptualization: PL. Investigation: ZY, PL, RR, GA, XL. Data curation: ZY, RR, XL, PL, ZZ, SC. Funding acquisition: PL. Writing - initial: ZY, PL. Writing - Review and Editing: PL, ZY, GA, RR, XL.

Data and Code Availability

GSHA v1.0 is openly available at https://doi.org/10.5281/zenodo.8090704https://doi.org/10.5281/zenodo.8090704 and https://doi.org/10.5281/zenodo.10127757. The codes involved in the workflow to generating GSHA will be available upon reasonable requests to the corresponding author.

Competing interests

The authors declare no conflict of interest.

Acknowledgements

This study is supported by the National Key Research and Development Program (2022YFF0801303), the Yunnan Provincial Basic Research Project-Science and Technology Special Project of Southwest United Graduate School (#305107035054), the Natural Science Foundation of China (42371481, 42175178), and the Fundamental Research Funds for the Central Universities, to Peking University on "Numerical modelling and remote sensing of global river discharge" (#7100604136).

References

Addor, N., Do, H. X., Alvarez-Garreton, C., Coxon, G., Fowler, K., & Mendoza, P. A. (2020). Large-sample hydrology: recent progress, guidelines for new datasets and grand challenges. *Hydrological Sciences Journal-Journal Des Sciences Hydrologiques*, *65*(5), 712-725. https://doi.org/10.1080/02626667.2019.1683182

Addor, N., Nearing, G., Prieto, C., Newman, A. J., Le Vine, N., & Clark, M. P. (2018). A ranking of hydrological signatureshydrologicalsignatures based on their predictability in space. *Water Resources Research*, *54*(11), 8792-8812.

Addorhttps://doi.org/10.1029/2018WR022606Addor, N., Newman, A. J., Mizukami, N., & Clark, M. P. (2017). The CAMELS data set: catchment attributes and meteorology for large-sample studies.

Hydrology and Earth System Sciences, *21*(10), 5293-5313. https://doi.org/10.5194/hess-21-5293-2017

Aerts, J. P., Hut, R. W., van de Giesen, N. C., Drost, N., van Verseveld, W. J., Weerts, A. H., & Hazenberg, P. (2022). Large-sample assessment of varying spatial resolution on the streamflow estimates of the wflow_sbm hydrological model. *Hydrology and Earth System Sciences*, *26*(16), 4407-4430., https://doi.org/10.5194/hess-26-4407-2022.

AghaKouchak, A., Chiang, F., Huning, L. S., Love, C. A., Mallakpour, I., Mazdiyasni, O., Moftakhari, H., Papalexiou, S. M., Ragno, E., & Sadegh, M. (2020). Climate Extremes and Compound Hazards in a Warming World. *Annual Review of Earth and Planetary Sciences, Vol 48, 2020*, *48*, 519-548. <Go to ISI>://WOS:000613951000021https://doi.org/10.1146/annurev-earth-071719-055228

Alvarez-Garreton, C., Mendoza, P. A., Boisier, J. P., Addor, N., Galleguillos, M., Zambrano-Bigiarini, M., Lara, A., Puelma, C., Cortes, G., Garreaud, R., McPhee, J., & Ayala, A. (2018). The CAMELS-CL dataset: catchment attributes and meteorology for large sample studies - Chile dataset. *Hydrology and Earth System Sciences*, *22*(11), 5817-5846. https://doi.org/10.5194/hess-22-5817-2018

ArcticNET 2022 ArcticNET V1.0 (available at: https://russia-arcticnet.sr.unh.edu/)

Arsenault, R., Brissette, F., Martel, J.-L., Troin, M., Lévesque, G., Davidson-Chaput, J., Gonzalez, M. C., Ameli, A., & Poulin, A. (2020). A comprehensive, multisource database for hydrometeorological modeling of 14,425 North American watersheds. *Scientific Data*, *7*(1), 243. https://doi.org/10.1038/s41597-020-00583-2

Australian Bureau of Meteorology 2022 Australian Bureau of Meteorology (available at: www.bom.gov.au/)www.bom.gov.au/)

Banasik, K., and Hejduk, L. "Long-term changes in runoff from a small agricultural catchment." Soil and Water Research 7, no. 2 (2012): 64-72. https://doi.org/10.1007/s10661-006-0769-2

Beck, H. E., van Dijk, A. I., De Roo, A., Miralles, D. G., McVicar, T. R., Schellekens, J., & Bruijnzeel, L. A. (2016). Global-scale regionalization of hydrologic model parameters. *Water Resources Research*, *52*(5), 3599-3622. https://doi.org/10.1002/2015WR018247

Beck, H. E., Van Dijk, A. I., Levizzani, V., Schellekens, J., Miralles, D. G., Martens, B., & De Roo, A. (2017). MSWEP: 3-hourly 0.25 global gridded precipitation (1979–2015) by merging gauge, satellite, and reanalysis data. *Hydrology and Earth System Sciences*, *21*(1), 589-615. https://doi.org/10.5194/hess-21-589-2017

Beck, H. E., Wood, E. F., Pan, M., Fisher, C. K., Miralles, D. G., Van Dijk, A. I., McVicar, T. R., & Adler, R. F. (2019). MSWEP V2 global 3-hourly 0.1 precipitation: methodology and quantitative assessment. *Bulletin of the American Meteorological Society*, *100*(3), 473-500. https://doi.org/10.1175/BAMS-D-17-0138.1

Belvederesi, C., Zaghloul, M. S., Achari, G., Gupta, A., & Hassan, Q. K. (2022). Modelling river flow in cold and ungauged regions: A review of the purposes, methods, and challenges. *Environmental Reviews*, *30*(1), 159-173. https://doi.org/10.1139/er-2021-0043

Benke, K. K., Lowell, K. E., & Hamilton, A. J. (2008). Parameter uncertainty, sensitivity analysis and prediction error in a water-balance hydrological model. *Mathematical and Computer Modelling*, *47*(11-12), 1134-1149. https://doi.org/10.1016/j.mcm.2007.05.017

Beven, K. J., & Alcock, R. E. (2012). Modelling everything everywhere: a new approach to decision-making for water management under uncertainty. *Freshwater Biology*, *57*, 124-132.

771 https://doi.org/10.1111/j.1365-2427.2011.02592.x

772 Bourdin, D. R., Fleming, S. W., & Stull, R. B. (2012). Streamflow modelling: a primer on applications,
773 approaches and challenges. *Atmosphere-Ocean*, *50*(4), 507-536.
774 https://doi.org/10.1080/07055900.2012.734276

775 Brazil National Water Agency 2022 National water and sanitation agency (ANA) Agência Nac Águas E
776 Saneam. Básico ANA (available at: www.gov.br/ana/en/national_water_agency)

777 Brugnara, Y., Good, E., Squintu, A. A., van der Schrier, G., & Brönnimann, S. (2019). The EUSTACE
778 global land station daily air temperature dataset. *Geoscience Data Journal*, *6*(2), 189-204.
779 https://doi.org/10.1002/gdj3.81

780 Brun, P., Zimmermann, N. E., Hari, C., Pellissier, L., & Karger, D. N. (2022). Global climate-related
781 predictors at kilometer resolution for the past and future. *Earth System Science Data*, *14*(12),
782 5573-5603. https://doi.org/10.5194/essd-14-5573-2022

783 Brunner, M. I., Slater, L., Tallaksen, L. M., & Clark, M. (2021). Challenges in modeling and predicting
784 floods and droughts: A review. *Wiley Interdisciplinary Reviews: Water*, *8*(3), e1520.
785 https://doi.org/10.1002/wat2.1520

786 Burges, S. J. (1998). Streamflow prediction: capabilities, opportunities, and challenges. *Hydrologic
787 Sciences: Taking Stock and Looking Ahead*, *5*, 101-134.

788 Canada National Water Data Archive 2022 National water data archive HYDAT (available at:
789 www.canada.ca/en/environment-climate-change/services/water-
790 overview/quantity/monitoring/survey/data-products-services/national-archive-hydat.html)

791 Chagas, V. B., Chaffe, P. L., Addor, N., Fan, F. M., Fleischmann, A. S., Paiva, R. C., & Siqueira, V. A.
792 (2020). CAMELS-BR: hydrometeorological time series and landscape attributes for 897
793 catchments in Brazil. *Earth System Science Data*, *12*(3), 2075-2096.
794 https://doi.org/10.5194/essd-12-2075-2020

795 Chen, X., Jiang, L., Luo, Y., ~~&~~and Liu, J~~. (2023).~~.: A global streamflow indices time series dataset for
796 large-sample hydrological analyses on streamflow regime (until ~~2021).~~2022), *Earth* ~~*System*~~
797 ~~*Science*~~*Syst. Sci. Data* ~~*Discussions*, ~~, 15, 4463–4479, https://doi.org/10.5194/essd-15-4463-
798 2023~~, 1–18.~~

799 Chile Center for Climate and Resilience Research 2022 Center for climate and resilience research CR2 |
800 Chilean research center on climate, climate change and resilience (available at: www.cr2.cl/eng/)

801 Cho, K., & Kim, Y. (2022). Improving streamflow prediction in the WRF-Hydro model with LSTM
802 networks. *Journal of Hydrology*, *605*, 127297. https://doi.org/10.1016/j.jhydrol.2021.127297

803 Clark, M. P., Vogel, R. M., Lamontagne, J. R., Mizukami, N., Knoben, W. J., Tang, G., Gharari, S., Freer,
804 J. E., Whitfield, P. H., & Shook, K. R. (2021). The abuse of popular performance metrics in
805 hydrologic modeling. *Water Resources Research*, *57*(9), e2020WR029001.
806 https://doi.org/10.1029/2020WR029001

807 Claverie, M., Matthews, J. L., Vermote, E. F., & Justice, C. O. (2016). A 30+ year AVHRR LAI and
808 FAPAR climate data record: Algorithm description and validation. *Remote Sensing*, *8*(3), 263.
809 https://doi.org/10.3390/rs8030263

810 Coxon, G., Addor, N., Bloomfield, J. P., Freer, J., Fry, M., Hannaford, J., Howden, N. J., Lane, R., Lewis,
811 M., & Robinson, E. L. (2020). CAMELS-GB: hydrometeorological time series and landscape
812 attributes for 671 catchments in Great Britain. *Earth System Science Data*, *12*(4), 2459-2483.
813 https://doi.org/10.5194/essd-12-2459-2020

814 Olivier Delaigue, ~~O.,~~Pierre Brigode, ~~P.,~~Vazken Andréassian, ~~V.,~~Charles Perrin, ~~C.,~~Pierre Etchevers, ~~P.,~~

815 ~~Soubeyroux, J.-M., Janet, B., & Nans, A. (2022).~~et al.. CAMELS-FR: A large sample
816 hydroclimatic dataset for France to explore hydrological diversity and support model
817 benchmarking. *IAHS-2022 Scientific Assembly*, ~~575.~~May 2022, Montpellier, France. hal-
818 03687235

819 Do, H. X., Gudmundsson, L., Leonard, M., & Westra, S. (2018). The Global Streamflow Indices and
820 Metadata Archive (GSIM) - Part 1: The production of a daily streamflow archive and metadata.
821 *Earth System Science Data*, *10*(2). https://doi.org/10.5194/essd-10-765-2018

822 Duan, Q., Schaake, J., Andréassian, V., Franks, S., Goteti, G., Gupta, H., Gusev, Y., Habets, F., Hall, A.,
823 & Hay, L. (2006). Model Parameter Estimation Experiment (MOPEX): An overview of science
824 strategy and major results from the second and third workshops. *Journal of Hydrology*, *320*(1-
825 2), 3-17. https://doi.org/10.1016/j.jhydrol.2005.07.031

826 Fang, Y., Huang, Y., Qu, B., Zhang, X., Zhang, T., & Xia, D. (2022). Estimating the Routing Parameter
827 of the Xin'anjiang Hydrological Model Based on Remote Sensing Data and Machine Learning.
828 *Remote Sensing*, *14*(18), 4609. https://doi.org/10.3390/rs14184609

829 Fowler, K. J. A., Acharya, S. C., Addor, N., Chou, C. C., & Peel, M. C. (2021). CAMELS-AUS:
830 hydrometeorological time series and landscape attributes for 222 catchments in Australia. *Earth
831 System Science Data*, *13*(8), 3847-3867. https://doi.org/10.5194/essd-13-3847-2021

832 Friedl, M. A., Sulla-Menashe, D., Tan, B., Schneider, A., Ramankutty, N., Sibley, A., & Huang, X. (2010).
833 MODIS Collection 5 global land cover: Algorithm refinements and characterization of new
834 datasets. *Remote Sensing of Environment*, *114*(1), 168-182.
835 https://doi.org/10.1016/J.RSE.2009.08.016

836 Friedl, M., D. Sulla-Menashe. MCD12Q1 MODIS/Terra+Aqua Land Cover Type Yearly L3 Global 500m
837 SIN Grid V006. 2019, distributed by NASA EOSDIS Land Processes DAAC,
838 https://doi.org/10.5067/MODIS/MCD12Q1.006.

839 Gelaro, R., McCarty, W., Suárez, M. J., Todling, R., Molod, A., Takacs, L., Randles, C. A., Darmenov,
840 A., Bosilovich, M. G., & Reichle, R. (2017). The modern-era retrospective analysis for research
841 and applications, version 2 (MERRA-2). *Journal of Climate*, *30*(14), 5419-5454.
842 https://doi.org/10.1175/JCLI-D-16-0758.1

843 Global Modeling and Assimilation Office (GMAO) (2015), inst3_3d_asm_Cp: MERRA-2 3D IAU State,
844 Meteorology Instantaneous 3-hourly (p-coord, 0.625x0.5L42), version 5.12.4, Greenbelt, MD,
845 USA: Goddard Space Flight Center Distributed Active Archive Center (GSFC DAAC),
846 https://doi.org/10.5067/VJAFPLI1CSIV.

847 Gudmundsson, L., Do, H. X., Leonard, M., & Westra, S. (2018). The Global Streamflow Indices and
848 Metadata Archive (GSIM) - Part 2: Quality control, time-series indices and homogeneity
849 assessment. *Earth System Science Data*, *10*(2). https://doi.org/10.5194/essd-10-787-2018

850 Gupta, H. V., Perrin, C., Bloschl, G., Montanari, A., Kumar, R., Clark, M., & Andreassian, V. (2014).
851 Large-sample hydrology: a need to balance depth with breadth. *Hydrology and Earth System
852 Sciences*, *18*(2), 463-477. https://doi.org/10.5194/hess-18-463-2014

853 Hao, Z., Jin, J., Xia, R., Tian, S., Yang, W., Liu, Q., Zhu, M., Ma, T., Jing, C., & Zhang, Y. (2021). CCAM:
854 China catchment attributes and meteorology dataset. *Earth System Science Data*, *13*(12), 5591-
855 5616. https://doi.org/10.5194/essd-13-5591-2021

856 Henck, A. C., Montgomery, D. R., Huntington, K. W., & Liang, C. (2010). Monsoon control of effective
857 discharge, Yunnan and Tibet. *Geology, 38*(11), 975-978. https://doi.org/10.1130/G31444.1

858 Hersbach, H., Bell, B., Berrisford, P., Hirahara, S., Horányi, ~~A~~Á., Muñoz-Sabater, J., Nicolas, J. P.,

Peubey, C., Radu, R., & Schepers, D., Simmons, A. J., Soci, C., Abdalla, S., Abellan, X., Balsamo, G., Bechtold, P., Biavati, G., Bidlot, J., Bonavita, M., . . . Thépaut, J. (2020). The ERA5 global reanalysis. *Quarterly Journal of the Royal Meteorological Society*, 146(730), 1999-2049.

Hrachowitz 2049. https://doi.org/10.1002/qj.3803Hrachowitz, M., Savenije, H., Blöschl, G., McDonnell, J., Sivapalan, M., Pomeroy, J., Arheimer, B., Blume, T., Clark, M., & Ehret, U. (2013). A decade of Predictions in Ungauged Basins (PUB)—a review. *Hydrological sciences journal*, 58(6), 1198-1255. https://doi.org/10.1080/02626667.2013.803183

Hu, D., Cao, S., Chen, S., Deng, L., & Feng, N. (2017). Monitoring spatial patterns and changes of surface net radiation in urban and suburban areas using satellite remote-sensing data. *International Journal of Remote Sensing*, 38(4), 1043-1061. https://doi.org/10.1080/01431161.2016.1275875

Huang, Yinghuai (2020): High spatiotemporal resolution mapping of global urban change from 1985 to 2015. figshare. Dataset. https://doi.org/10.6084/m9.figshare.11513178.v1

Immerzeel, W., and, & Droogers, P. (2008). Calibration of a distributed hydrological model based on satellite evapotranspiration. *Journal of Hydrology*, 349(3-4), 411-424. https://doi.org/10.1016/j.jhydrol.2007.11.017

India Water Resources Information System 2022 India Water Resources Information System (available at: https://indiawris.gov.in/wris/#/)

Japanese Water Information System 2022 Ministry of Land, Infrastructure, Transport and Tourism (available at: www.mlit.go.jp/en/)

Kauffeldt, A., Halldin, S., Rodhe, A., Xu, C.-Y., & Westerberg, I. K. (2013). Disinformative data in large-scale hydrological modelling. *Hydrology and Earth System Sciences*, 17(7), 2845-2857. https://doi.org/10.5194/hess-17-2845-2013

Klingler, C., Schulz, K., & Herrnegger, M. (2021). LamaH-CE: LArge-SaMple DAta for Hydrology and Environmental Sciences for Central Europe. *Earth System Science Data*, 13(9), 4529-4565. https://doi.org/10.5194/essd-13-4529-2021

Kovács, G. (1984). Proposal to construct a coordinating matrix for comparative hydrology. *Hydrological sciences journal*, 29(4), 435-443. https://doi.org/10.1080/02626668409490961

Kratzert, F., Klotz, D., Shalev, G., Klambauer, G., Hochreiter, S., & Nearing, G. (2019a). Benchmarking a catchment-aware long short-term memory network (LSTM) for large-scale hydrological modeling. *Hydrol. Earth Syst. Sci. Discuss*, 2019, 1-32. https://doi.org/10.5194/hess-2019-368

Kratzert, F., Klotz, D., Shalev, G., Klambauer, G., Hochreiter, S., & Nearing, G. (2019b). Towards learning universal, regional, and local hydrological behaviors via machine learning applied to large-sample datasets. *Hydrology and Earth System Sciences*, 23(12), 5089-5110. https://doi.org/10.5194/hess-23-5089-2019, 2019.

Kratzert, F., Nearing, G., Addor, N., Erickson, T., Gauch, M., Gilon, O., Gudmundsson, L., Hassidim, A., Klotz, D., & Nevo, S. (2023). Caravan-A global community dataset for large-sample hydrology. *Scientific Data*, 10(1), 61. https://doi.org/10.1038/s41597-023-01975-w

Lehner, B., Messager, M. L., Korver, M. C., & Linke, S. (2022). Global hydro-environmental lake characteristics at high spatial resolution. *Scientific Data*, 9(1), 351. https://doi.org/10.1038/s41597-022-01425-z

Li, B., Rodell, M., Kumar, S., Beaudoing, H. K., Getirana, A., Zaitchik, B. F., de Goncalves, L. G.,

Cossetin, C., Bhanja, S., & Mukherjee, A. (2019). Global GRACE data assimilation for groundwater and drought monitoring: Advances and challenges. *Water Resources Research*, *55*(9), 7564-7586. https://doi.org/10.1029/2018WR024618

Lin, P., Rajib, M. A., Yang, Z. L., Somos-Valenzuela, M., Merwade, V., Maidment, D. R., Wang, Y., & Chen, L. (2018). Spatiotemporal evaluation of simulated evapotranspiration and streamflow over Texas using the WRF-Hydro-RAPID modeling framework. *JAWRA Journal of the American Water Resources Association*, *54*(1), 40-54. https://doi.org/10.1111/1752-1688.12585

Lin, P. R., Pan, M., Beck, H. E., Yang, Y., Yamazaki, D., Frasson, R., David, C. H., Durand, M., Pavelsky, T. M., Allen, G. H., Gleason, C. J., & Wood, E. F. (2019). Global Reconstruction of Naturalized River Flows at 2.94 Million Reaches. *Water Resources Research*, *55*(8), 6499-6516. https://doi.org/10.1029/2019wr025287

Lin, P. R., Pan, M., Wood, E. F., Yamazaki, D., & Allen, G. H. (2021). A new vector-based global river network dataset accounting for variable drainage density. *Scientific Data*, *8*(1). https://doi.org/ARTN 2810.1038/s41597-021-00819-9

Linke, S., Lehner, B., Ouellet Dallaire, C., Ariwi, J., Grill, G., Anand, M., Beames, P., Burchard-Levine, V., Maxwell, S., & Moidu, H. (2019). Global hydro-environmental sub-basin and river reach characteristics at high spatial resolution. *Scientific Data*, *6*(1), 283. https://doi.org/10.1038/s41597-019-0300-6

Liu, X., Huang, Y., Xu, X., Li, X., Li, X., Ciais, P., Lin, P., Gong, K., Ziegler, A. D., & Chen, A. (2020). High-spatiotemporal-resolution mapping of global urban change from 1985 to 2015. *Nature Sustainability*, *3*(7), 564-570. https://doi.org/10.1038/s41893-020-0521-x

Lu, J., Wang, G., Chen, T., Li, S., Hagan, D. F. T., Kattel, G., Peng, J., Jiang, T., & Su, B. (2021). A harmonized global land evaporation dataset from model-based products covering 1980–2017. *Earth System Science Data*, *13*(12), 5879-5898. https://doi.org/10.5194/essd-13-5879-2021

Lucas-Borja, M. E., Carrà, B. G., Nunes, J. P., Bernard-Jannin, L., Zema, D. A., Zimbone, S. M., (2020) Impacts of land-use and climate changes on surface runoff in a tropical forest watershed (Brazil), Hydrological Sciences Journal, 65:11, 1956-1973, https://doi.org/10.1016/j.catena.2006.04.015

Martens, B., Miralles, D. G., Lievens, H., Van Der Schalie, R., De Jeu, R. A., Fernández-Prieto, D., Beck, H. E., Dorigo, W. A., & Verhoest, N. E. (2017). GLEAM v3: Satellite-based land evaporation and root-zone soil moisture. *Geoscientific Model Development*, *10*(5), 1903-1925. https://doi.org/10.5194/gmd-10-1903-2017

Merchant, C. J., Paul, F., Popp, T., Ablain, M., Bontemps, S., Defourny, P., Hollmann, R., Lavergne, T., Laeng, A., & De Leeuw, G. (2017). Uncertainty information in climate data records from Earth observation. *Earth System Science Data*, *9*(2), 511-527. https://doi.org/10.5194/essd-9-511-2017

Miralles, D. G., Holmes, T., De Jeu, R., Gash, J., Meesters, A., & Dolman, A. (2011). Global land-surface evaporation estimated from satellite-based observations. *Hydrology and Earth System Sciences*, *15*(2), 453-469. https://doi.org/10.5194/hess-15-453-2011

Muñoz-Sabater, J., Dutra, E., Agustí-Panareda, A., Albergel, C., Arduini, G., Balsamo, G., Boussetta, S., Choulga, M., Harrigan, S., & Hersbach, H. (2021). ERA5-Land: A state-of-the-art global reanalysis dataset for land applications. *Earth System Science Data*, *13*(9), 4349-4383. https://doi.org/10.5194/essd-13-4349-2021

Muñoz Sabater, J., (2019): ERA5-Land hourly data from 1981 to present. Copernicus Climate Change Service (C3S) Climate Data Store (CDS)., 10.24381/cds.e2161bac

947 Nandi, S., & Reddy, M. J. (2022). An integrated approach to streamflow estimation and flood inundation
948   mapping using VIC, RAPID and LISFLOOD-FP. *Journal of Hydrology*, *610*, 127842.
949   https://doi.org/10.1016/j.jhydrol.2022.127842

950 Newman, A. J., Clark, M. P., Sampson, K., Wood, A., Hay, L. E., Bock, A., Viger, R. J., Blodgett, D.,
951   Brekke, L., Arnold, J. R., Hopson, T., & Duan, Q. (2015). Development of a large-sample
952   watershed-scale hydrometeorological data set for the contiguous USA: data set characteristics
953   and assessment of regional variability in hydrologic model performance. *Hydrology and Earth*
954   *System Sciences*, *19*(1), 209-223. https://doi.org/10.5194/hess-19-209-2015

955 Niraula, R., Meixner, T., & Norman, L. M. (2015). Determining the importance of model calibration for
956   forecasting absolute/relative changes in streamflow from LULC and climate changes. *Journal*
957   *of Hydrology*, *522*, 439-451. https://doi.org/10.1016/j.jhydrol.2015.01.007

958 Qu, S., Wang, L., Lin, A., Zhu, H., & Yuan, M. (2018). What drives the vegetation restoration in Yangtze
959   River basin, China: climate change or anthropogenic factors? *Ecological Indicators*, *90*, 438-
960   450. https://doi.org/10.1016/j.ecolind.2018.03.029

961 Razavi, T., & Coulibaly, P. (2013). Streamflow prediction in ungauged basins: review of regionalization
962   methods. *Journal of hydrologic engineering*, *18*(8), 958-975.
963   https://doi.org/10.1061/(ASCE)HE.1943-5584.0000690

964 Ren, K., Fang, W., Qu, J., Zhang, X., & Shi, X. (2020). Comparison of eight filter-based feature selection
965   methods for monthly streamflow forecasting–three case studies on CAMELS data sets. *Journal*
966   *of Hydrology*, *586*, 124897. https://doi.org/10.1016/j.jhydrol.2020.124897

967 Riggs, R. M., Allen, G. H., Wang, J., Pavelsky, T. M., Gleason, C. J., David, C. H., & Durand, M. (2023).
968   Extending global river gauge records using satellite observations. *Environmental Research*
969   *Letters*. https://doi.org/10.1088/1748-9326/acd407

970 Schaake, J., Cong, S., and Duan, Q. (2006). "U.S. MOPEX
971 DATA SET". United States. https://www.osti.gov/servlets/purl/899413.Schmidt, A. H., Montgomery, D.
972   R., Huntington, K. W., & Liang, C. (2011). The question of communist land degradation: new
973   evidence from local erosion and basin-wide sediment yield in Southwest China and Southeast
974   Tibet. *Annals of the Association of American Geographers, 101*(3), 477-496.
975   https://doi.org/10.1080/00045608.2011.560059

976 Schreiner-McGraw, A. P., & Ajami, H. (2020). Impact of uncertainty in precipitation forcing data sets
977   on the hydrologic budget of an integrated hydrologic model in mountainous terrain. *Water*
978   *Resources Research*, *56*(12), e2020WR027639. https://doi.org/10.1029/2020WR027639

979 Singer, M. B., Asfaw, D. T., Rosolem, R., Cuthbert, M. O., Miralles, D. G., MacLeod, D., Quichimbo, E.
980   A., & Michaelides, K. (2021). Hourly potential evapotranspiration at 0.1 resolution for the
981   global land surface from 1981-present. *Scientific Data*, *8*(1), 224.
982   https://doi.org/10.1038/s41597-021-01003-9

983 Spain Anuario de Aforos 2022 Anuario de Aforos—Anuario de Aforos Digital—datos.gob.es (available
984   at: http://datos.gob.es/es/catalogo/e00125801-anuario-de-aforos/resource/4836b826-e7fd-
985   4a41-950c-89b4eaea0279)

986 Sörensson, A. A., & Ruscica, R. C. (2018). Intercomparison and uncertainty assessment of nine
987   evapotranspiration estimates over South America. *Water Resources Research*, *54*(4), 2891-2908.
988   https://doi.org/10.1002/2017WR021682

989 Tang, G., Clark, M. P., & Papalexiou, S. M. (2022). EM-Earth: The ensemble meteorological dataset for
990   planet Earth. *Bulletin of the American Meteorological Society*, *103*(4), E996-E1018.

991   https://doi.org/10.1175/BAMS-D-21-0106.1

992   Tang, G., Clark, M., Papalexiou, S. (2022) EM-Earth: The Ensemble Meteorological Dataset for Planet

993   Earth. Federated Research Data Repository. https://doi.org/10.20383/102.0547

994   Tang, G., Clark, M. P., Knoben, W. J. M., Liu, H., Gharari, S., Arnal, L., et al. (2023). The impact of

995   meteorological forcing uncertainty on hydrological modeling: A global analysis of cryosphere

996   basins. *Water Resources Research, 59,* e2022WR033767. https://doi.org/10.1029/2022WR0337

997   Thackeray, C. W., Hall, A., Norris, J., & Chen, D. (2022). Constraining the increased frequency of global

998   precipitation extremes under warming. *Nature Climate Change*, *12*(5), 441-448.

999   https://doi.org/10.1038/s41558-022-01329-1

1000   Thailand Royal Irrigation Department 2022 RID River Discharge Data (available at: http://hydro.iis.u-

1001   tokyo.ac.jp/GAME-T/GAIN-T/routine/rid-river/disc_d.html)

1002   The Global Runoff Data Centre 2022 The global runoff data centre GRDC Data Portal (available at:

1003   https://portal.grdc.bafg.de/applications/public.html?publicuser=PublicUser)

1004   Ukhurebor, K. E., Azi, S. O., Aigbe, U. O., Onyancha, R. B., & Emegha, J. O. (2020). Analyzing the

1005   uncertainties between reanalysis meteorological data and ground measured meteorological data.

1006   *Measurement*, *165*, 108110. https://doi.org/10.1016/j.measurement.2020.108110

1007   U.S.   Geological   Survey   2019   Gages   Through   the   Ages   (available   at:

1008   https://labs.waterdata.usgs.gov/visualizations/gages-through-the-

1009   ages)https://labs.waterdata.usgs.gov/visualizations/gages-through-the-ages)

1010   Velpuri, N. M., and G. B. Senay. "Analysis of long-term trends (1950–2009) in precipitation, runoff and

1011   runoff coefficient in major urban watersheds in the United States." Environmental Research

1012   Letters 8, no. 2 (2013): 024020. https://doi.org/10.1088/1748-9326/8/2/024020

1013   Vermote, Eric; NOAA CDR Program. (2019): NOAA Climate Data Record (CDR) of AVHRR Leaf Area

1014   Index (LAI) and Fraction of Absorbed Photosynthetically Active Radiation (FAPAR), Version

1015   5.   [LAI].   NOAA   National   Centers   for   Environmental   Information.

1016   https://doi.org/10.7289/V5TT4P69.

1017   Wang, J., Walter, B. A., Yao, F., Song, C., Ding, M., Maroof, A. S., Zhu, J., Fan, C., McAlister, J. M., &

1018   Sikder, S. (2022). GeoDAR: georeferenced global dams and reservoirs dataset for bridging

1019   attributes   and   geolocations.   *Earth   System   Science   Data*,   *14*(4),   1869-1899.

1020   https://doi.org/10.5194/essd-14-1869-2022

1021   Wilby, R. L., & Dessai, S. (2010). Robust adaptation to climate change. *Weather, 65(7), 180–185.*

1022   https://doi.org/10.1002/wea.543

1023   Xiong, J., Yin, J., Guo, S., He, S., & Chen, J. (2022). Annual runoff coefficient variation in a changing

1024   environment: A global perspective. *Environmental Research Letters*, *17*(6), 064006.

1025   https://doi.org/10.1088/1748-9326/ac62ad

1026   Yamazaki, D., Ikeshima, D., Sosa, J., Bates, P. D., Allen, G. H., & Pavelsky, T. M. (2019). MERIT Hydro:

1027   a high-resolution global hydrography map based on latest topography dataset. *Water Resources*

1028   *Research*, *55*(6), 5053-5073. https://doi.org/10.1029/2019WR024873

1029   Yamazaki, D., Ikeshima, D., Tawatari, R., Yamaguchi, T., O'Loughlin, F., Neal, J. C., Sampson, C. C.,

1030   Kanae, S., & Bates, P. D. (2017). A high-accuracy map of global terrain elevations. *Geophysical*

1031   *Research Letters*, *44*(11), 5844-5853. https://doi.org/10.1002/2017GL072874

1032   Yang, L., Yang, Y., Villarini, G., Li, X., Hu, H., Wang, L., Blöschl, G., & Tian, F. (2021). Climate more

1033   important for Chinese flood changes than reservoirs and land use. *Geophysical Research Letters*,

1034   *48*(11), e2021GL093061. https://doi.org/10.1029/2021GL093061

1035 Yang, L., Yang, Y. X., Villarini, G., Li, X., Hu, H. C., Wang, L. C., Bloschl, G., & Tian, F. Q. (2021).
1036 ~~Climate More Important for Chinese Flood Changes Than Reservoirs and Land Use.~~
1037 ~~*Geophysical Research Letters*, *48*(11). https://doi.org/ARTN~~
1038 ~~e2021GL09306110.1029/2021GL093061~~

1039 Yin, Z., Lin, P., Riggs, R., Allen, G. H., Lei, X., Zheng, Z., & Cai, S. (2023). A Synthesis of Global
1040 Streamflow characteristics, Hydrometeorology, and catchment Attributes (GSHA) for Large
1041 Sample River-Centric Studies (1.0) [Data set]. Zenodo.
1042 ~~https://doi.org/10.5281/zenodo.8090704~~https://doi.org/10.5281/zenodo.8090704

1043 Ziyun Yin, Peirong Lin, Ryan Riggs, George H. Allen, Xiangyong Lei, Ziyan Zheng, & Siyu Cai. (2023).
1044 A Synthesis of Global Streamflow characteristics, Hydrometeorology, and catchment Attributes
1045 (GSHA) for Large Sample River-Centric Studies V1.1 (1.1) [Data set]. Zenodo.
1046 https://doi.org/10.5281/zenodo.10127757

1047 Zaitchik, B. F., Rodell, M., & Reichle, R. H. (2008). Assimilation of GRACE terrestrial water storage
1048 data into a land surface model: Results for the Mississippi River basin. *Journal of*
1049 *Hydrometeorology*, *9*(3), 535-548. https://doi.org/10.1175/2007jhm951.1

1050 Zhang, J., Lin, P., Gao, S., & Fang, Z. (2020). Understanding the re-infiltration process to simulating
1051 streamflow in North Central Texas using the WRF-hydro modeling system. *Journal of*
1052 *Hydrology*, *587*, 124902. https://doi.org/10.1016/j.jhydrol.2020.124902

1053 Zhang, J., Wang, T., & Ge, J. (2015). Assessing vegetation cover dynamics induced by policy-driven
1054 ecological restoration and implication to soil erosion in southern China. *PLoS One*, *10*(6),
1055 e0131352. https://doi.org/10.1371/journal.pone.0131352

1056 Zhang, S., Zhou, L., Zhang, L., Yang, Y., Wei, Z., Zhou, S., Yang, D., Yang, X., Wu, X., & Zhang, Y.
1057 (2022). Reconciling disagreement on global river flood changes in a warming climate. *Nature*
1058 *Climate Change*, 1-8. https://doi.org/10.1038/s41558-022-01539-7

1059 Zhang, Y., & Liang, S. (2014). Changes in forest biomass and linkage to climate and forest disturbances
1060 over Northeastern China. *Global change biology*, *20*(8), 2596-2606.
1061 https://doi.org/10.1111/gcb.12588

1062 Zhang, Y., Zheng, H., Zhang, X., Leung, L. R., Liu, C., Zheng, C., Guo, Y., Chiew, F. H., Post, D., &
1063 Kong, D. (2023). Future global streamflow declines are probably more severe than previously
1064 estimated. *Nature Water*, 1-11. https://doi.org/10.1038/s44221-023-00030-7

1065
1066